

Collisional transfer of population and orientation in NaK

C. M. Wolfe,^{1,a)} S. Ashman,^{1,b)} J. Bai,² B. Beser,² E. H. Ahmed,² A. M. Lyyra,² and J. Huennekens^{1,c)}¹*Department of Physics, 16 Memorial Dr. East, Lehigh University, Bethlehem, Pennsylvania 18015, USA*²*Department of Physics, Temple University, Philadelphia, Pennsylvania 19122-6082, USA*

(Received 21 December 2010; accepted 17 March 2011; published online 2 May 2011)

Collisional satellite lines with $|\Delta J| \leq 58$ have been identified in recent polarization spectroscopy V-type optical-optical double resonance (OODR) excitation spectra of the Rb₂ molecule [H. Salami *et al.*, Phys. Rev. A **80**, 022515 (2009)]. Observation of these satellite lines clearly requires a transfer of population from the rotational level directly excited by the pump laser to a neighboring level in a collision of the molecule with an atomic perturber. However to be observed in polarization spectroscopy, the collision must also partially preserve the angular momentum orientation, which is at least somewhat surprising given the extremely large values of ΔJ that were observed. In the present work, we used the two-step OODR fluorescence and polarization spectroscopy techniques to obtain quantitative information on the transfer of population and orientation in rotationally inelastic collisions of the NaK molecules prepared in the $2(A)^1\Sigma^+(v' = 16, J' = 30)$ rovibrational level with argon and potassium perturbers. A rate equation model was used to study the intensities of these satellite lines as a function of argon pressure and heat pipe oven temperature, in order to separate the collisional effects of argon and potassium atoms. Using a fit of this rate equation model to the data, we found that collisions of NaK molecules with potassium atoms are more likely to transfer population and destroy orientation than collisions with argon atoms. Collisions with argon atoms show a strong propensity for population transfer with $\Delta J = \text{even}$. Conversely, collisions with potassium atoms do not show this $\Delta J = \text{even}$ propensity, but do show a propensity for $\Delta J = \text{positive}$ compared to $\Delta J = \text{negative}$, for this particular initial state. The density matrix equations of motion have also been solved numerically in order to test the approximations used in the rate equation model and to calculate fluorescence and polarization spectroscopy line shapes. In addition, we have measured rate coefficients for broadening of NaK $3^1\Pi \leftarrow 2(A)^1\Sigma^+$ spectral lines due to collisions with argon and potassium atoms. Additional broadening, due to velocity changes occurring in rotationally inelastic collisions, has also been observed. © 2011 American Institute of Physics. [doi:10.1063/1.3575234]

I. INTRODUCTION

From an experimental point of view, alkali diatomic molecules provide an ideal environment for basic quantum mechanical studies, since transitions between electronic states lie in the visible and near infrared, thereby allowing high-resolution tunable lasers to be used for excitation. In addition, alkali molecules are of intense current interest for cooling and trapping studies and in the production of molecular Bose condensates. There is a need for basic spectroscopic data on alkali molecules; such studies are usually carried out at much higher temperatures and densities, and collisional satellite lines can greatly expand spectral line datasets.^{1,2} Collisional processes are also responsible for the redistribution of population among various energy levels and for the destruction of laser-induced orientation and alignment. It is the object of the present work to separately measure rate coefficients for the transfer of population and orientation in collisions of heteronuclear alkali

molecules with atomic perturbers. Specifically, this work uses fluorescence and polarization spectroscopy to investigate the transfer of population and partial preservation of orientation in rotationally inelastic collisions of NaK molecules with either argon or potassium atom perturbers.

Measurements of rate coefficients for collisions between alkali molecules and atomic partners in which population is transferred from one rovibrational level to a neighboring level, typically referred to as “vibrotationally inelastic collisions,” have been carried out in a number of laboratories since the pioneering work of Bergmann and Demtröder,^{3–5} Ottinger *et al.*,⁶ and Ottinger and Poppe.⁷ Bergmann and Demtröder investigated collisions of noble gas atoms with Na₂ molecules in the $B^1\Pi_u$ state and determined cross sections for rotationally and vibrationally inelastic transitions, while Ottinger and co-workers studied similar collisions in the Li₂ $B^1\Pi_u$ system. Later, Brunner *et al.*⁸ studied rotationally inelastic collisions in the Na₂ ($A^1\Sigma_u^+$)–Xe system, while Scott *et al.*⁹ measured rate constants for rotationally inelastic collisions from levels of initial rotational angular momenta $J_i = 8, 22,$ and 42 to levels of final angular momenta $J_f = J_i + \Delta J$ for Li₂($A^1\Sigma_u^+$) + Xe, Ar, and Ne. This latter study was expanded to include both vibrationally as well as rotationally

^{a)}Present address: Army Research Laboratory, RDRL-WMP-A, Aberdeen Proving Ground, Maryland 21005-5066, USA.

^{b)}Present address: Department of Physics and Astronomy, University of Wisconsin–Stevens Point, Stevens Point, Wisconsin 54481, USA.

^{c)}Author to whom correspondence should be addressed. Electronic mail: jph7@lehigh.edu.

inelastic collisions,^{10–13} wherein an interesting propensity rule $\Delta J = -4\Delta v$ for the most probable collisional transitions in this molecule was discovered. A theoretical interpretation of these data was given by McCaffery.¹⁴ The rate coefficients for Li_2 ($A^1\Sigma_u^+$) + Li were measured using similar techniques.¹⁵ In addition, rate coefficients for vibrationally inelastic Li_2 ($A^1\Sigma_u^+$)–noble gas collisions were determined systematically for a wide range of initial vibrational levels using the same experimental setup,^{16,17} and these were compared to calculations using the Li_2 ($A^1\Sigma_u^+$) + Ne *ab initio* potential energy surface of Ref. 18. Vibrotationally inelastic collisions have also been investigated in the ultracold regime where they are expected to have significant effects on cooling.^{19–22}

Rotationally inelastic collisions have been observed in polarization spectroscopy as far back as 1976 by Teets *et al.*²³ Since polarization spectroscopy signals cannot be observed without angular momentum orientation (or alignment), this implies that at least some orientation (or alignment) can survive an inelastic collision. The loss of angular momentum orientation of a molecule in a collision has most commonly been studied by observing the polarization of fluorescence emitted by excited molecules in the initial and final levels.^{24,25} The relative M_J level orientation can be determined from the ratio of circularly polarized light emitted by molecules in the collisionally populated level compared to that emitted by molecules in the directly populated level. Alexander and Davis²⁶ and Derouard²⁷ developed detailed theoretical treatments which were compared to the experimental results of Refs. 24, 28, and 8. This work demonstrated that a propensity exists for preserving $\theta = \cos^{-1}(\hat{J} \cdot \hat{z})$ rather than for preserving M_J in the collision.

In recent years various novel techniques have been developed to probe the orientation of a molecule following a collision. These include the observation of fluorescence from crossed beams (one beam is the molecular sample under investigation and the other is the collision partner),^{29,30} polarization spectroscopy wherein the depolarization of the molecule is probed after the collision by a pulsed laser,^{23,31–39} and Zeeman quantum beat spectroscopy.^{40,41} A comparison between these latter two methods was made in Ref. 42 and excellent agreement was found.

The current work was initially motivated by our recent observation of rotationally inelastic collisions in Rb_2 using polarization spectroscopy with cw lasers in a heat pipe oven.¹ In that work, a particular rovibrational level of the molecular ground state $1(X)^1\Sigma_g^+(v'', J'')$ was oriented by a circularly polarized pump laser tuned to a specific transition $1(B)^1\Pi_u(v', J') \leftarrow 1(X)^1\Sigma_g^+(v'', J'')$, and then a linearly polarized probe laser utilized that lower state orientation to map out various $1(b)^3\Pi_u(v_b, J') \sim 1(A)^1\Sigma_u^+(v_A, J')$ levels as its frequency was scanned across $1(b)^3\Pi_u(v_b, J') \sim 1(A)^1\Sigma_u^+(v_A, J') \leftarrow 1(X)^1\Sigma_g^+(v'', J'')$ transitions. A great number of collisional lines $1(b)^3\Pi_u(v_b, J' + \Delta J) \sim 1(A)^1\Sigma_u^+(v_A, J' + \Delta J) \leftarrow 1(X)^1\Sigma_g^+(v'', J'' + \Delta J)$ were also observed in the spectra, suggesting that not only population, but also orientation, was being transferred fairly efficiently from the labeled state $1(X)^1\Sigma_g^+(v'', J'')$ to the neighboring states $1(X)^1\Sigma_g^+(v'', J'' + \Delta J)$ in the collision. What was particularly surprising

was the large amount of angular momentum that could be transferred in the collision. Figure 1 shows an example where the level $J_{\text{initial}} = 71$ was tagged by the pump laser and collisional lines associated with all even ΔJ values down to $J_{\text{final}} = 13$ (corresponding to $|\Delta J| = 58$) were observed.^{1,43} Despite these very large changes of J , a measurable fraction of the initial M_J level orientation must be retained in the rotationally inelastic collision.

In Ref. 1, it was not possible to separate the effects of population and orientation transfer from each other. Therefore, it is the aim of the current work to utilize the techniques of polarization spectroscopy and laser-induced fluorescence spectroscopy in order to separately determine quantitative information on the rate coefficients for population and orientation transfer in collisions between NaK molecules and atomic collision partners, as well as to separately determine the different effects of argon and potassium atoms as the collision partner. A principal difference between the present work and that reported in Refs. 1 and 23 is that here we study collisions involving excited molecules [$2(A)^1\Sigma^+$] rather than ground state molecules. Since the excited state lifetime is much shorter than the effective ground state lifetime (determined by transit relaxation), we are not able to observe such large values of ΔJ (transitions involving $|\Delta J|$ up to 12 were observed in the present work, and we quantitatively studied transitions up to $|\Delta J| = 4$). However, by studying excited state collisions we could carry out laser-induced fluorescence as well as polarization spectroscopy measurements, and it is the combination of these techniques that allows the effects of population and orientation transfer to be examined separately. In addition, use of the heteronuclear molecule NaK allowed us to observe transitions with $|\Delta J| = \text{odd}$, thereby exposing some interesting propensity rules.

This manuscript is organized as follows. In Sec. II, we describe the experimental setup used in this work. Section III provides a derivation of the polarization spectroscopy lineshape function, and a description of the empirical rate equation model used in the analysis of our experimental data. Section IV presents our results for the collisional rate coefficients for the rotationally inelastic collisions $2(A)^1\Sigma^+(v', J') \rightarrow 2(A)^1\Sigma^+(v', J' + \Delta J)$ and for the fraction of the initial orientation that is lost in the collision. We also present results for the collisional broadening of the NaK $3^1\Pi(v = 7, J = 29) \leftrightarrow 2(A)^1\Sigma^+(v' = 16, J' = 30)$ transition by argon and potassium perturbers, since this provides a good estimate of collisional dephasing rates for this and similar transitions in alkali molecules. Finally, Sec. V presents our conclusions.

II. EXPERIMENT

The experimental setup is shown in Fig. 2. A mixture of sodium and potassium is contained in a six-arm cross-type heat-pipe oven, along with argon buffer gas. The heat-pipe oven can be operated in either the “heat-pipe” mode or the “oven” mode. In the former,⁴⁴ the temperature is sufficient to produce an alkali atom vapor pressure that is equal to the argon vapor pressure. In these circumstances, the argon is excluded from the central heated zone of the oven.⁴⁴ In the “oven” mode, the temperature is lower than that re-

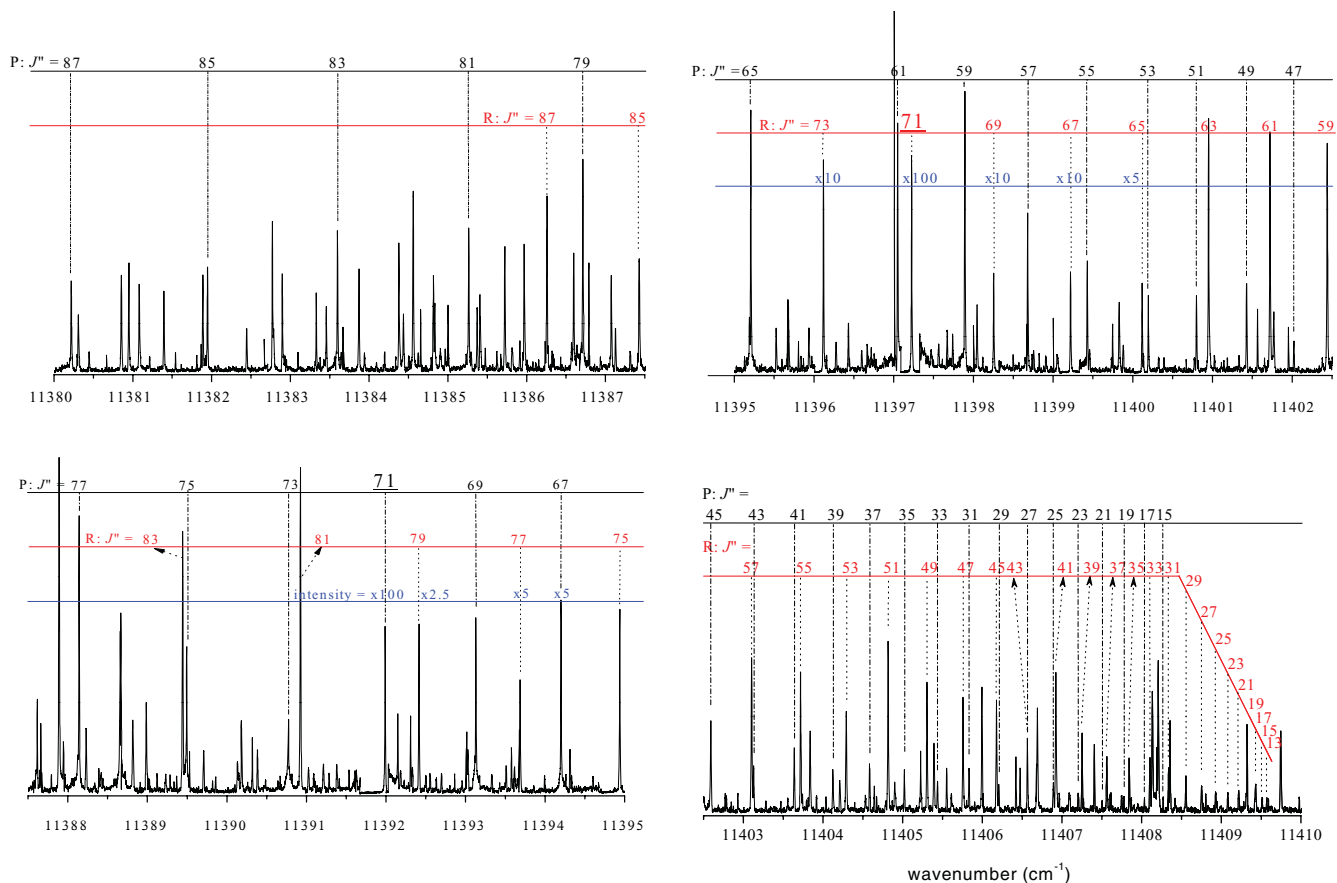


FIG. 1. $\text{Rb}_2 A^1\Sigma_u^+ \leftarrow X^1\Sigma_g^+$ spectrum recorded using polarization spectroscopy showing collisional transfer of population and orientation with $|\Delta J|$ up to 58. The pump laser was tuned to the $B^1\Pi_u(v' = 2, J' = 70) \leftarrow X^1\Sigma_g^+(v'' = 0, J'' = 71)$ transition, creating orientation in the $X^1\Sigma_g^+(v'' = 0, J'' = 71)$ level. The probe laser was scanned over the various $A^1\Sigma_u^+(v', J') \leftarrow X^1\Sigma_g^+(v'' = 0, J'')$ transitions. Signals could be identified for collisionally populated ground state levels with $13 \leq J''_{\text{final}} \leq 87$.

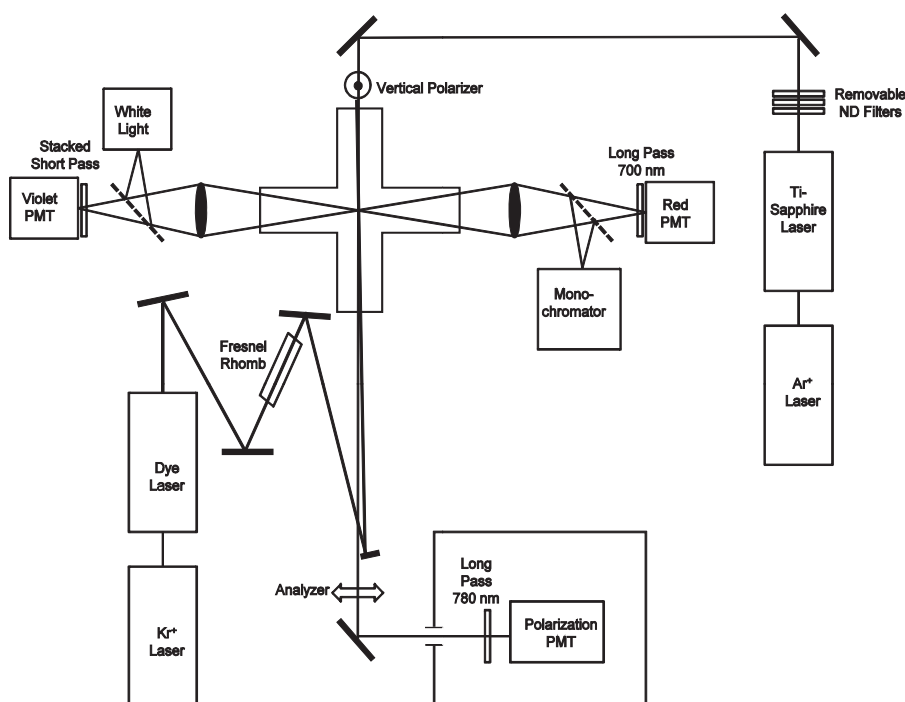


FIG. 2. Experimental setup. The white light and monochromator are used in measurements of atomic potassium density using the absorption equivalent width technique.

quired to produce an alkali vapor pressure equal to the argon pressure, so the alkali and argon vapors mix in the central region. In either case, some fraction (typically less than 1%) of the alkali atoms combine to form diatomic molecules K_2 , NaK , and Na_2 .

We use the optical-optical double resonance technique^{45–62} to study collisions of excited NaK molecules with alkali and argon atoms. A Coherent 699–29 single-mode cw tunable dye laser (the pump laser) using the dye LD700 produces 140–470 mW of power in the range 725–775 nm ($12\,900$ – $13\,800$ cm^{-1}) when pumped with 3–5 W from a Kr^+ laser. The dye laser excites NaK molecules to the $2(A)^1\Sigma^+(v' = 16, J' = 30)$ rovibrational level when tuned to the $2(A)^1\Sigma^+(v' = 16, J' = 30) \leftarrow 1(X)^1\Sigma^+(v'' = 0, J'' = 29)$ transition. The $2(A)^1\Sigma^+(v' = 16, J' = 30)$ level directly excited by the pump laser, as well as neighboring levels, $2(A)^1\Sigma^+(v' = 16, J' = 30 + \Delta J)$, populated by collisions, are then probed by a counterpropagating Coherent 899–29 single-mode Ti:Sapphire laser (the probe laser), which is pumped by 10 W from an Ar^+ ion laser. The Ti:Sapphire laser produces 100–850 mW of power in the 800–920 nm wavelength range using the midwave optics set. Because the narrow-band pump laser only excites molecules in a specific velocity group, the OODR method is intrinsically Doppler-free, and homogeneous linewidths can be resolved.

In the present work, we utilize both polarization spectroscopy and laser-induced fluorescence spectroscopy in this OODR configuration. The pump laser beam is circularly polarized by the Fresnel rhomb (see Fig. 2) and creates an anisotropic distribution of population in the M_J sublevels (net orientation) of both the $2(A)^1\Sigma^+(v' = 16, J' = 30)$ and $1(X)^1\Sigma^+(v'' = 0, J'' = 29)$ levels. The probe laser frequency is scanned across the direct $3^1\Pi(v = 6 \text{ or } 7, J = 29) \leftarrow 2(A)^1\Sigma^+(v' = 16, J' = 30)$ transition, as well as several collisional $3^1\Pi(v = 6 \text{ or } 7, J = 29 + \Delta J) \leftarrow 2(A)^1\Sigma^+(v' = 16, J' = 30 + \Delta J)$ transitions that are observed as weaker satellite lines adjacent to the direct line. In the fluorescence technique (see Fig. 3), the direct and collisional lines are observed by monitoring violet fluorescence back to the ground state, $3^1\Pi(v = 6 \text{ or } 7, J) \rightarrow 1(X)^1\Sigma^+(v'', J'' = J \pm 1)$, in the side direction using a filtered, free-standing PMT (labeled “Violet PMT” in Fig. 2) as the probe laser is scanned over the various probe transitions. The PMT anode current is sent to a lock-in amplifier (Stanford Research Systems model SR850), and the pump laser is modulated by a mechanical chopper so that phase-sensitive detection can be employed. Since a particular set of probe laser transitions all correspond to neighboring rotational transitions within the same vibrational band, whose Franck–Condon factors are all approximately equal, it is a good approximation to assume that the fluorescence signals provide an accurate measure of the relative populations in the directly excited $2(A)^1\Sigma^+(v' = 16, J' = 30)$ and collisionally populated $2(A)^1\Sigma^+(v' = 16, J' = 30 + \Delta J)$ intermediate state levels. (We have also verified that to within measurement uncertainties the collisional to direct line fluorescence intensity ratios are independent of probe laser power.) In the polarization technique, the probe laser power is reduced to ~ 1 – 2 mW. The probe beam is sent through a pair of linear

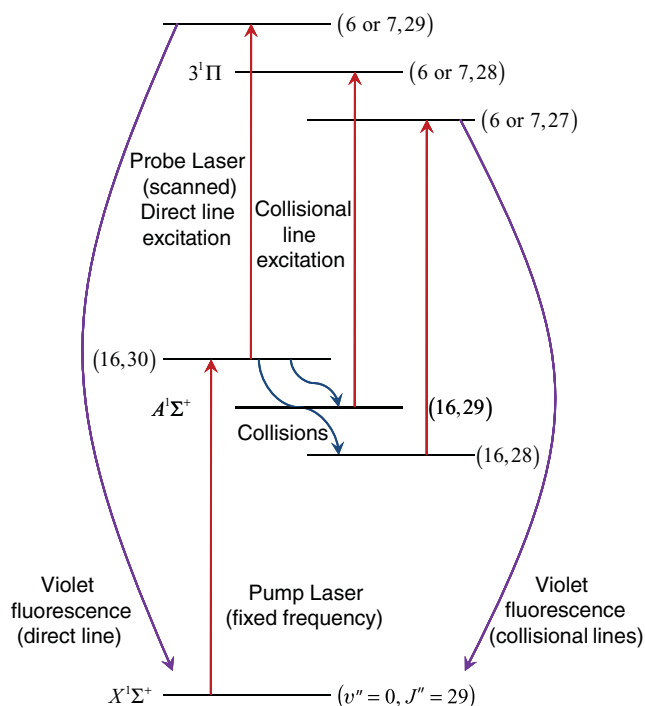


FIG. 3. Energy level diagram for fluorescence experiment. The frequency of the pump laser is fixed to line center of the $A^1\Sigma^+(v' = 16, J' = 30) \leftarrow X^1\Sigma^+(v'' = 0, J'' = 29)$ transition. The frequency of the probe laser is scanned over the “direct” line $3^1\Pi(v = 6 \text{ or } 7, J = 29) \leftarrow A^1\Sigma^+(v' = 16, J' = 30)$ and over the “collisional” lines $3^1\Pi(v = 6 \text{ or } 7, J = 29 + \Delta J) \leftarrow A^1\Sigma^+(v' = 16, J' = 30 + \Delta J)$. Excitation is detected by monitoring total violet $3^1\Pi \rightarrow X^1\Sigma^+$ fluorescence.

polarizers, one located before and one after the heat pipe oven, and then to a detector (labeled “Polarization PMT” in Fig. 2). Again the PMT anode current is processed by the lock-in amplifier and the lock-in output is digitized and recorded on a computer. When the probe frequency is off resonance, the second linear polarizer completely blocks the probe beam from reaching the detector (assuming perfect polarizers). However, when the probe laser frequency is tuned to a transition sharing either the upper level, the lower level, or both levels with the pump laser transition, then the net orientation of these levels causes the probe laser polarization to acquire a slight ellipticity, resulting in some transmission through the second polarizer. It is straightforward to show that the measured polarization signals are proportional to the product of the population in the initial level of the probe transmission and the net orientation of that level (see Sec. III B). Thus a comparison of the polarization and fluorescence signals allows us to separate the effects of collisional transfer of orientation from collisional transfer of population. Figure 4 shows an example of fluorescence and polarization spectroscopy signals recorded under identical circumstances (except probe laser power).

The direct and collisional lines are recorded as functions of both argon and potassium densities. This is accomplished by changing the buffer gas pressure (in order to vary argon density) and heat pipe oven temperature (in order to vary potassium density). The densities of other species in the

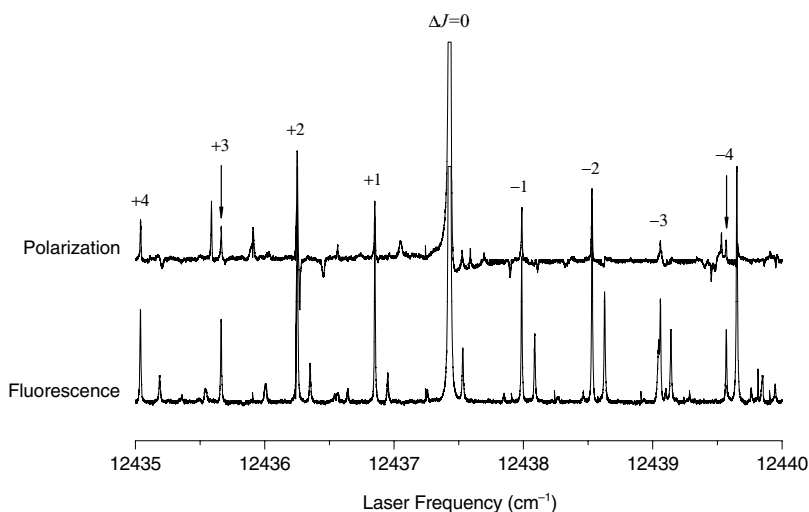


FIG. 4. A comparison of fluorescence (lower trace) and polarization spectroscopy (upper trace) signals showing collisional lines corresponding to $\Delta J = \pm 1, \pm 2, \pm 3, \pm 4$. The direct lines ($\Delta J = 0$) go far off scale in both traces.

vapor (Na, Na₂, K₂, and NaK) are much smaller than those of argon and potassium and thus can, to a good approximation, be neglected in the analysis. In the present work, the potassium partial pressure is calculated using the vapor pressure formula of Nesmeyanov,⁶³ adjusted as described in Sec. IV, while the argon partial pressure is then determined by subtracting the potassium partial pressure from the total gas pressure measured in the heat pipe oven using a capacitance manometer attached to the gas inlet. Densities are obtained from pressures using the ideal gas law.

III. THEORY

In this section a description of the polarization spectroscopy lineshape function is given. This is followed by a description of the empirical rate equation models used to determine rate coefficients for collisional transfer of population and orientation from measured ratios of collisional to direct line intensities obtained in the fluorescence and polarization spectroscopy experiments.

A. Polarization spectroscopy lineshapes

The technique of polarization spectroscopy was first introduced in Ref. 64. This technique provides an extremely sensitive means for measuring spectral line positions and is described in detail in Ref. 65. In polarization spectroscopy, as implemented in the current experiment, a circularly polarized laser beam (the pump) is used to create a net orientation (anisotropic distribution of M_J sublevels) in particular rovibrational levels of molecules in the vapor. The counterpropagating probe laser beam is sent through a vertical linear polarizer, then through the vapor, and finally through a crossed (horizontal) linear polarizer, before reaching a detector. When tuned to a transition involving one of the oriented levels, the polarization of the probe laser beam acquires some degree of ellipticity and thus is partially transmitted by the final linear polarizer. In order to understand the polarization spectroscopy excitation spectra,

it is useful to discuss the derivation of the lineshape function. For this, we follow the basic derivation of Ref. 65.

We begin by considering a linearly polarized laser beam, propagating along the \hat{z} axis with its polarization axis defined as \hat{x} . Thus the electric field at $z = 0$ can be written as

$$\mathbf{E}_{\text{initial}} = E_0 \hat{x} e^{-i\omega t}. \quad (1)$$

We can break this up into equal components of left and right circular polarization states by writing:

$$\mathbf{E}_{\text{initial}} = \frac{E_0}{\sqrt{2}} \left\{ \frac{1}{\sqrt{2}} (\hat{x} + i\hat{y}) e^{-i\omega t} + \frac{1}{\sqrt{2}} (\hat{x} - i\hat{y}) e^{-i\omega t} \right\}, \quad (2)$$

where $(\hat{x} + i\hat{y})$ indicates the left circular polarized component and $(\hat{x} - i\hat{y})$ indicates the right circular polarized component. As this beam passes through a vapor of length L and the two windows of the oven, each of thickness d , that have different absorption coefficients and refractive indices for left and right circular polarized light, the two components of the beam will be affected differently. We write out the refractive indices of the windows and vapor as

$$n_w^\pm = \text{Re}[n_w^\pm] + i\text{Im}[n_w^\pm] \quad (3)$$

$$n_v^\pm = \text{Re}[n_v^\pm] + i\text{Im}[n_v^\pm], \quad (4)$$

where w indicates window, v indicates vapor, and $+$ or $-$ refers to the response to left or right circular polarization, respectively. The electric field after passing through the vapor and windows is then given by

$$\begin{aligned} \mathbf{E} = \frac{E_0}{2} \left\{ (\hat{x} + i\hat{y}) \exp \left\{ i \left(\frac{2d\omega}{c} \text{Re}[n_w^+] + \frac{L\omega}{c} \text{Re}[n_v^+] - \omega t \right) \right\} \right. \\ \times \exp \left\{ - \left(\frac{2d\omega}{c} \text{Im}[n_w^+] + \frac{L\omega}{c} \text{Im}[n_v^+] \right) \right\} \\ + (\hat{x} - i\hat{y}) \exp \left\{ i \left(\frac{2d\omega}{c} \text{Re}[n_w^-] + \frac{L\omega}{c} \text{Re}[n_v^-] - \omega t \right) \right\} \\ \left. \times \exp \left\{ - \left(\frac{2d\omega}{c} \text{Im}[n_w^-] + \frac{L\omega}{c} \text{Im}[n_v^-] \right) \right\} \right\}. \quad (5) \end{aligned}$$

We simplify the notation by using $b^\pm \equiv (2d\omega/c) \operatorname{Re}[n_w^\pm]$, $\beta^\pm \equiv (2d\omega/c) \operatorname{Im}[n_w^\pm]$, $n^\pm \equiv (L\omega/c) \operatorname{Re}[n_v^\pm]$, and $\alpha^\pm \equiv (L\omega/c) \operatorname{Im}[n_v^\pm]$, and further simplify by setting $b \equiv (b^+ + b^-)/2$, $\Delta b \equiv (b^+ - b^-)/2$, $\beta \equiv (\beta^+ + \beta^-)/2$, $\Delta\beta \equiv (\beta^+ - \beta^-)/2$, $n \equiv (n^+ + n^-)/2$, $\Delta n \equiv (n^+ - n^-)/2$, $\alpha \equiv (\alpha^+ + \alpha^-)/2$, and $\Delta\alpha \equiv (\alpha^+ - \alpha^-)/2$ (these definitions are slightly different from those used in Ref. 65). This allows us to write the x and y components of the electric field as

$$E_x = \frac{E_0}{2} e^{i(b+n-\omega t)} e^{-(\beta+\alpha)} \{ e^{i(\Delta b+\Delta n)} e^{-(\Delta\beta+\Delta\alpha)} + e^{-i(\Delta b+\Delta n)} e^{\Delta\beta+\Delta\alpha} \}, \quad (6)$$

$$E_y = \frac{E_0 i}{2} e^{i(b+n-\omega t)} e^{-(\beta+\alpha)} \{ e^{i(\Delta b+\Delta n)} e^{-(\Delta\beta+\Delta\alpha)} - e^{-i(\Delta b+\Delta n)} e^{\Delta\beta+\Delta\alpha} \}. \quad (7)$$

We now allow this electric field to pass through a nearly crossed polarizer, with its transmission axis y' oriented at a very small angle θ with respect to the y axis, so the transmitted electric field amplitude is the projection of the incident electric field onto the transmission axis of the polarizer:

$$E_t = \mathbf{E} \cdot \hat{\mathbf{y}}' = -E_x \sin\theta + E_y \cos\theta. \quad (8)$$

Using $e^{\pm i\theta} = \cos\theta \pm i \sin\theta$, we obtain

$$E_t = i \frac{E_0}{2} e^{i(b+n-\omega t)} e^{-(\beta+\alpha)} \{ e^{i(\Delta b+\Delta n+\theta)} e^{-(\Delta\beta+\Delta\alpha)} - e^{-i(\Delta b+\Delta n+\theta)} e^{\Delta\beta+\Delta\alpha} \}. \quad (9)$$

Now, the transmitted intensity is $I_t = c\varepsilon_0 |E_t|^2$. Using this, along with some familiar trigonometric identities, and defining $\theta' \equiv \theta + \Delta b$, we obtain

$$I_t = \frac{I_0}{2} e^{-2(\beta+\alpha)} \{ \cosh(2\Delta\beta) \cosh(2\Delta\alpha) + \sinh(2\Delta\beta) \sinh(2\Delta\alpha) - \cos(2\Delta n) \cos(2\theta') + \sin(2\Delta n) \sin(2\theta') \}. \quad (10)$$

Assuming that the uncrossing angle θ and the differences in left and right circular absorption coefficients and birefringences are all small quantities, we expand the trigonometric and hyperbolic functions and retain terms only through second order;

$$I_t = \frac{I_0}{2} e^{-2(\beta+\alpha)} \{ 1 + 2(\Delta\beta)^2 + 2(\Delta\alpha)^2 + 4\Delta\beta\Delta\alpha - 1 + 2\Delta n^2 + 2(\theta')^2 + 4\Delta n\theta' \}. \quad (11)$$

In addition, because the polarizers are not perfect, a small fraction $I/I_0 \equiv \xi$ of the intensity of the “wrong” polarization $\mathbf{E} \cdot \hat{\mathbf{x}}' = E_x \cos\theta + E_y \sin\theta$ is also transmitted to the detector. Assuming ξ is also a small quantity and retaining terms only through second order in small quantities just adds a background term 2ξ inside the curly brackets of Eq. (11). Thus we arrive at the final equation for the transmitted intensity,

$$I_t = I_0 e^{-2(\beta+\alpha)} \{ \xi + (\theta')^2 + \Delta\beta^2 + 2\Delta\beta\Delta\alpha + 2\Delta n\theta' + \Delta\alpha^2 + \Delta n^2 \}. \quad (12)$$

The probe laser beam only interacts with molecules in the velocity group excited by the pump laser, so the probe absorption profile will be Lorentzian in nature, and we can write the vapor circular dichroism term as

$$\Delta\alpha(\omega) = \frac{\Delta\alpha_0}{1+x^2}, \quad \text{with } x \equiv \frac{\omega_0 - \omega}{\Gamma/2}, \quad (13)$$

where $\Delta\alpha_0$ is the circular dichroism at line-center ($\omega = \omega_0$). Because the absorption and refractive index are related by the dispersion relation of Kronig and Kramers, we can write the vapor circular birefringence in terms of the line-center dichroism $\Delta\alpha_0$:

$$\Delta n(\omega) = \frac{\Delta\alpha_0 x}{1+x^2}. \quad (14)$$

Using Eqs. (13) and (14) in Eq. (12), we arrive at the final polarization spectroscopy lineshape function,

$$I_t = I_0 e^{-2(\beta+\alpha)} \left\{ \xi + (\theta')^2 + \Delta\beta^2 + 2\Delta\beta \frac{\Delta\alpha_0}{1+x^2} + 2\theta' \frac{\Delta\alpha_0 x}{1+x^2} + \left(\frac{\Delta\alpha_0}{1+x^2} \right)^2 + \left(\frac{\Delta\alpha_0 x}{1+x^2} \right)^2 \right\}. \quad (15)$$

We note that Eq. (15) is almost identical to Eq. (2.50) of Ref. 65, but corrects a couple of minor typographical errors in the latter.

In Eq. (15), the leading terms ξ , $(\theta')^2$, and $\Delta\beta^2$ are background terms that are constant in laser frequency. As discussed in Ref. 65, the dispersion term can be minimized by adjusting the analyzer crossing angle θ to cancel out the window birefringence Δb (i.e., setting $\theta' = 0$). Because the window terms are generally quite large compared to the vapor terms, the Lorentzian squared and dispersion squared terms will be small compared to the first order Lorentzian and dispersion terms. Thus the main contributor to the polarization spectroscopy lineshape is the first order Lorentzian term involving the difference in absorption by the vapor of the left and right circularly polarized components of the probe beam, multiplied by the window dichroism. Conversely, one can adjust the pressure on the oven windows to make $\Delta\beta \approx 0$ but slightly uncross the polarizer axes. This results in dispersion shaped lines proportional to θ' .

In the present experiment θ is adjusted to make $\theta' = 0$ so that the polarization spectroscopy lineshapes we observed were mostly Lorentzian. The remaining background terms $\xi + \Delta\beta^2$ in Eq. (15) are suppressed by the use of phase-sensitive detection. Because $\Delta\alpha_0$ has opposite sign for P lines ($J_{\text{upper}} - J_{\text{lower}} = -1$) and R lines ($J_{\text{upper}} - J_{\text{lower}} = +1$), these two types of transitions can be easily distinguished in the spectra, thus greatly simplifying the assignment of lines.

B. Empirical model to describe collisional population and orientation transfer

In order to extract rate coefficients for collisional transfer of population and orientation from our measured collisional to direct line intensity ratios, we have developed a rate equation model for the fluorescence and polarization spectroscopy experiments. We assume that the NaK molecule is

prepared in an initial state [$2(A)^1\Sigma^+(v' = 16, J' = 30)$] labeled state 1' (note that we use single primes to designate intermediate state levels in our OODR pump/probe scheme), with an initial population and orientation created by the pump laser. The molecule can then undergo collisions with either argon or potassium atoms (we assume that these are the dominant species in the vapor and neglect collisions with the much less numerous sodium atoms and K_2 , NaK, and Na_2 molecules), which transfer some of the population and some of the initial orientation to a neighboring rovibrational level [$2(A)^1\Sigma^+(v' = 16, J' = 30 + \Delta J)$] labeled state 2'. Subsequent collisions can transfer population from state 2' back to state 1' (back transfer) or to any other neighboring or distant level (collisional quenching). Collisions can also cause additional decay of orientation for molecules in state 2'.

We begin by considering a model for the fluorescence ratios, which are only sensitive to population transfer. We write a rate equation for the steady-state population in state 2',

$$\dot{n}_{2'} = 0 = (k_{Ar}^{\Delta J} n_{Ar} + k_K^{\Delta J} n_K) n_{1'} - (k_{Ar}^Q n_{Ar} + k_K^Q n_K) n_{2'} - \Gamma n_{2'}, \quad (16)$$

where n_{Ar} and n_K are the argon and potassium number densities, $k_{Ar}^{\Delta J}$ and $k_K^{\Delta J}$ are the rate coefficients for the transfer of population from state 1' to state 2' in collisions with argon and potassium atoms, respectively, and k_{Ar}^Q and k_K^Q are the quenching rates, describing the loss of population from state 2' after the initial collision. Γ is the rate for radiative decay from state 2'. In general, the collisional transfer rate coefficients $k_{Ar}^{\Delta J}$ and $k_K^{\Delta J}$ will be different depending on which neighboring rotational level is represented by state 2', so we include the ΔJ superscript. However, since the quenching rates involve transitions to all neighboring and distant levels, we assume they are approximately constant with the rotational quantum number for state 2' (in this work we investigate collisions with $|\Delta J| \leq 4$, so we are assuming that the total collisional quenching rates for the levels $2(A)^1\Sigma^+(v' = 16, J' = 26 - 34)$ are approximately equal). Similarly, we assume that the radiative rates of state 1' and all states 2' under investigation are approximately equal. Therefore, the ratio $(I_{2'}^F/I_{1'}^F) \equiv R_F$ of violet $3^1\Pi(v = 6 \text{ or } 7, J) \rightarrow 1(X)^1\Sigma^+(v'', J'' = J \pm 1)$ fluorescence (collisional/direct) as the probe laser is scanned over transitions coupled to the collisionally populated state 2' [$3^1\Pi(v = 6 \text{ or } 7, J = 29 + \Delta J) \leftarrow 2(A)^1\Sigma^+(v' = 16, J' = 30 + \Delta J)$] and the directly excited state 1' [$3^1\Pi(v = 6 \text{ or } 7, J = 29) \leftarrow 2(A)^1\Sigma^+(v' = 16, J' = 30)$] is given to good approximation by the ratio of populations $n_{2'}/n_{1'}$ obtained by solving Eq. (16) in steady state,

$$R_F \equiv \frac{I_{2'}^F}{I_{1'}^F} = \frac{n_{2'}}{n_{1'}} = \frac{\frac{k_{Ar}^{\Delta J}}{\Gamma} n_{Ar} + \frac{k_K^{\Delta J}}{\Gamma} n_K}{1 + \frac{k_{Ar}^Q}{\Gamma} n_{Ar} + \frac{k_K^Q}{\Gamma} n_K}. \quad (17)$$

Equation (17) is used to model the ratios of collisional to direct line fluorescence intensities for each ΔJ .

For the polarization spectroscopy signals, we use the fact that the dominant term in the polarization spectroscopy lineshape function is the Lorentzian term proportional to the difference in absorption of left and right circular polarized

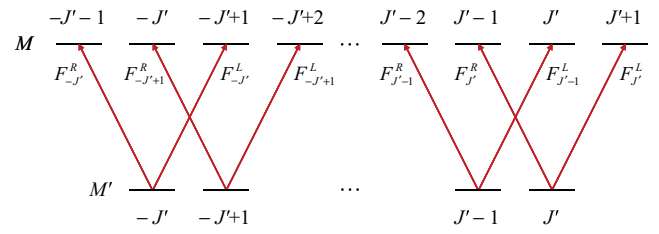


FIG. 5. Illustration of absorption of left and right circularly polarized light giving rise to the polarization spectroscopy signal. Arrows labeled F^L and F^R represent probe laser absorptions for left and right circularly polarized light, respectively, and the $F_{M'}^{L,R}$ represent absorption coefficients.

light by the vapor [i.e., the $\Delta\beta\Delta\alpha_0$ term in Eq. (15)]. Figure 5 is a schematic diagram showing the absorption of left ($\Delta M_J = +1$) and right ($\Delta M_J = -1$) circularly polarized light for transitions from different degenerate magnetic sublevels of the intermediate level (state 1' or state 2') to sublevels of the upper level in the probe transition [i.e., $3^1\Pi(v = 6 \text{ or } 7, J = 29) \leftarrow 2(A)^1\Sigma^+(v' = 16, J' = 30)$ for the direct line and $3^1\Pi(v = 6 \text{ or } 7, J = 29 + \Delta J) \leftarrow 2(A)^1\Sigma^+(v' = 16, J' = 30 + \Delta J)$ for the collisional lines in our experiment]. The intensities of the polarization spectroscopy lines can be represented by

$$\begin{aligned} I &\propto \sum(\text{Left absorptions}) - \sum(\text{Right absorptions}) \\ &= \sum_{M'=-J'}^{+J'} n_{M'} F_{M'}^L - \sum_{M'=-J'}^{+J'} n_{M'} F_{M'}^R \\ &= \sum_{M'=-J'}^{+J'} n_{M'} (F_{M'}^L - F_{M'}^R). \end{aligned} \quad (18)$$

Here the $F_{M'}^{L,R}$ coefficients are proportional to the absorption cross sections and thus represent the relative probability that the molecule will absorb either left or right circular polarized light, respectively, causing a transition from a specific M' magnetic sublevel in the intermediate level to a specific M magnetic sublevel in the upper level. These coefficients are given by Spano⁶⁶ for $^1\Sigma \rightarrow ^1\Sigma$ and $^1\Sigma \rightarrow ^1\Pi$ transitions. However, it should be noted that our $F_{M'}^{L,R}$ coefficients are the square of the F coefficients given in Ref. 66 divided by 2. Evaluation of the difference $(F_{M'}^L - F_{M'}^R)$ results in a function proportional to M' ,

$$F_{M'}^L - F_{M'}^R = f(J, J') M', \quad (19)$$

where $f(J, J')$ is a function that depends only on the rotational quantum numbers of the upper and lower levels of the probe transition and not on the M values of either state. The $f(J, J')$ values for $^1\Sigma \rightarrow ^1\Sigma$ and $^1\Sigma \rightarrow ^1\Pi$ transitions are given in Table I. Inserting Eq. (19) into Eq. (18), we obtain

$$I \propto f(J, J') \sum_{M'=-J'}^{+J'} M' n_{M'}. \quad (20)$$

The average value of M' (the orientation of the intermediate level of the probe transition) is given by $\langle M' \rangle = \sum_{M'=-J'}^{+J'} M' n_{M'} / \sum_{M'=-J'}^{+J'} n_{M'}$. Thus the sum in Eq. (20)

TABLE I. $f(J, J')$ values for ${}^1\Sigma \rightarrow {}^1\Sigma$ and ${}^1\Sigma \rightarrow {}^1\Pi$ transitions.

	$f(J, J')$	
	${}^1\Sigma \rightarrow {}^1\Sigma$	${}^1\Sigma \rightarrow {}^1\Pi$
R transitions $J = J' + 1$	$\frac{1}{(2J' + 1)}$	$\frac{(J' + 2)}{(J' + 1)(2J' + 1)}$
Q transitions $J = J'$		$\frac{1}{J'(J' + 1)}$
P transitions $J = J' - 1$	$-\frac{1}{(2J' + 1)}$	$-\frac{(J' - 1)}{J'(2J' + 1)}$

is equal to the orientation multiplied by the total population in that level,

$$I \propto f(J, J') \langle M' \rangle \sum_{M'=-J}^{+J} n_{M'}. \quad (21)$$

Assuming all other proportionality constants are the same (this is an excellent approximation since the transition frequencies, Franck–Condon factors, etc., are almost identical for neighboring rotational lines of the same vibrational band), we represent the ratio of the collisional (state 2') to direct (state 1') line polarization spectroscopy signals as

$$R_P \equiv \frac{I_{2'}^P}{I_{1'}^P} = \frac{f(J_2' - 1, J_2') \sum M_2' n_{M_2'}}{f(J_1' - 1, J_1') \sum M_1' n_{M_1'}} = \frac{f(J_2' - 1, J_2') \langle M_2' \rangle n_{2'}}{f(J_1' - 1, J_1') \langle M_1' \rangle n_{1'}}. \quad (22)$$

In this expression, we have used the fact that all probe transitions used in this work are *P* transitions ($J_{\text{upper}} - J_{\text{lower}} = -1$). Thus the ratio of collisional to direct line polarization signal strengths is essentially equal to the ratio of orientations times populations.

We can write a rate equation similar to Eq. (16) for the steady state orientation times population in state 2',

$$\begin{aligned} \frac{d}{dt} (\langle M_2' \rangle n_{2'}) = 0 = & k_{\text{Ar}}^{O, \Delta J} n_{\text{Ar}} \langle M_1' \rangle n_{1'} + k_{\text{K}}^{O, \Delta J} n_{\text{K}} \langle M_1' \rangle n_{1'} \\ & - g_{\text{Ar}} n_{\text{Ar}} \langle M_2' \rangle n_{2'} - g_{\text{K}} n_{\text{K}} \langle M_2' \rangle n_{2'} - \Gamma \langle M_2' \rangle n_{2'}. \end{aligned} \quad (23)$$

Here, $k_X^{O, \Delta J}$ is the rate coefficient for the transfer of population and orientation from state 1' to state 2' in a collision with species X, while g_X is the rate coefficient for the total decay of population or orientation from state 2' in collisions with species X. Solving Eq. (23) in steady state and combining with Eq. (22), we obtain

$$\begin{aligned} R_P \equiv \frac{I_{2'}^P}{I_{1'}^P} &= \frac{f(J_2' - 1, J_2') \langle M_2' \rangle n_{2'}}{f(J_1' - 1, J_1') \langle M_1' \rangle n_{1'}} \\ &= \frac{f(J_2' - 1, J_2') k_{\text{Ar}}^{O, \Delta J} n_{\text{Ar}} + k_{\text{K}}^{O, \Delta J} n_{\text{K}}}{f(J_1' - 1, J_1') \Gamma + g_{\text{Ar}} n_{\text{Ar}} + g_{\text{K}} n_{\text{K}}}. \end{aligned} \quad (24)$$

Next we separate the effects of population and orientation transfer by writing

$$k_X^{O, \Delta J} = k_X^{\Delta J} (1 - f_X^{\Delta J}), \quad (25)$$

$$g_X = k_X^Q + g_X', \quad (26)$$

where $k_X^{\Delta J}$ and k_X^Q are the same population transfer and quenching rate coefficients used in the fluorescence model, the parameter $f_X^{\Delta J}$ is the fraction of orientation lost in the collision that transfers population from state 1' to state 2', and the parameter g_X' is the rate coefficient for decay of orientation in collisions that do not result in a change in J . Inserting into Eq. (24) and rearranging, we arrive at the final expression for the ratio of collisional to direct line intensities as measured in the polarization spectroscopy experiment,

$$R_P = \frac{f(J_2' - 1, J_2') \frac{k_{\text{Ar}}^{\Delta J}}{\Gamma} (1 - f_{\text{Ar}}^{\Delta J}) n_{\text{Ar}} + \frac{k_{\text{K}}^{\Delta J}}{\Gamma} (1 - f_{\text{K}}^{\Delta J}) n_{\text{K}}}{f(J_1' - 1, J_1') \left(1 + \frac{k_{\text{Ar}}^Q + g_{\text{Ar}}'}{\Gamma} n_{\text{Ar}} + \frac{k_{\text{K}}^Q + g_{\text{K}}'}{\Gamma} n_{\text{K}} \right)}. \quad (27)$$

Preliminary fitting of the data showed that the $f_X^{\Delta J}$ and g_X' parameters were strongly correlated, especially for potassium collisions where $f_{\text{K}}^{\Delta J}$ is close to 1. Therefore, in fitting the data, we fix the parameter g_X' at the value

$$g_X' = \frac{1}{2} (f_X^{\Delta J = -1} k_X^{\Delta J = -1} + f_X^{\Delta J = +1} k_X^{\Delta J = +1}). \quad (28)$$

Thus we assume that the rate of decay of orientation in collisions that do not result in a change of J is equal to the average of the rates of decay of orientation in collisions that change J by plus or minus one unit. We do not believe this is a serious limitation of the model since g_X' turns out to be much smaller than k_X^Q (e.g., for the argon case where $f_{\text{Ar}}^{\Delta J}$ differs significantly from 1, $g_{\text{Ar}}' \approx 0$ when it was allowed to vary in the fit). We also note that Paterson *et al.*³⁹ found elastic depolarization rates that were generally smaller than rotationally inelastic population transfer rates for the OH($X^2\Pi$) + Ar system. Fixing g_X' at the value given by Eq. (28) allows us to fit the polarization intensity ratios to determine the probabilities for destruction of orientation ($f_{\text{Ar}}^{\Delta J}$ and $f_{\text{K}}^{\Delta J}$) for collisions corresponding to each value of ΔJ while the population transfer and quenching rate coefficients are determined primarily from fitting the fluorescence data.

IV. RESULTS AND DISCUSSION

A. Collisional transfer of population and orientation

We measured collisional to direct line intensity ratios, for $\Delta J = \pm 1, \pm 2, \pm 3$, and ± 4 , using both fluorescence and polarization spectroscopy at argon partial pressures between 0.1 and 7.7 Torr (argon densities between $1.5 \times 10^{15} \text{ cm}^{-3}$ and $1.4 \times 10^{17} \text{ cm}^{-3}$) and temperatures between 230 °C and 390 °C (potassium densities between $3.1 \times 10^{14} \text{ cm}^{-3}$ and $3.6 \times 10^{16} \text{ cm}^{-3}$). Some of the highest temperature data were recorded in heat pipe mode (where we assume that the argon pressure in the interaction region is zero). Tables 1 and 2 of the supplementary materials⁶⁷ provide lists of intensity ratios R_F and R_P measured for each ΔJ at each combination of argon and potassium densities. We note that because the spectral line widths of collisional lines are larger than the widths of the direct lines (see Sec. IV B), intensity ratios were determined, in all cases, by comparing areas rather than peak heights of the spectral lines.

TABLE II. Parameters obtained from empirical global fit to the data, using $\Gamma = 4.4 \times 10^7 \text{ s}^{-1}$.

ΔJ	Population transfer rate coefficients		Probability of destruction of orientation	
	Argon	Potassium	Argon	Potassium
	$k_{\text{Ar}}^{\Delta J} (10^{-11} \text{ cm}^3 \text{ s}^{-1})$	$k_{\text{K}}^{\Delta J} (10^{-10} \text{ cm}^3 \text{ s}^{-1})$	$f_{\text{Ar}}^{\Delta J}$	$f_{\text{K}}^{\Delta J}$
-4	8.4 ± 1.3	2.1 ± 0.5	0.67 ± 0.06	0.95 ± 0.04
-3	6.2 ± 1.0	2.6 ± 0.6	0.61 ± 0.09	0.88 ± 0.06
-2	19 ± 3	4.6 ± 1.1	0.42 ± 0.09	1.00 ± 0.18
-1	8.7 ± 1.4	6.2 ± 1.4	0.29 ± 0.12	0.98 ± 0.02
+1	6.9 ± 1.4	9.8 ± 1.9	0.28 ± 0.15	0.75 ± 0.08
+2	18 ± 3	8.8 ± 2.4	0.51 ± 0.09	0.85 ± 0.12
+3	4.5 ± 0.8	3.1 ± 0.8	0.37 ± 0.16	1.00 ± 0.11
+4	8.0 ± 1.3	1.8 ± 0.8	0.48 ± 0.10	1.00 ± 0.24
	Quenching rate coefficients			
	Argon		Potassium	
	$k_{\text{Ar}}^{\text{Q}} (10^{-9} \text{ cm}^3 \text{ s}^{-1})$		$k_{\text{K}}^{\text{Q}} (10^{-8} \text{ cm}^3 \text{ s}^{-1})$	
	1.0 ± 0.2		1.5 ± 0.4	

Because the quenching rate coefficients, k_X^{Q} , do not depend on ΔJ and are common to both the fluorescence and polarization intensity expressions [Eqs. (17) and (27)], we needed to fit all the data of both types and for all the different ΔJ values simultaneously. We also note that although the polarization ratios depend on $k_X^{\text{O},\Delta J}$, while the fluorescence ratios depend on $k_X^{\Delta J}$, these parameters are connected by Eq. (25) and the constraint that $0 \leq f_X^{\Delta J} \leq 1$. Thus we simultaneously fit the values of ratios R_F and R_P to Eqs. (17) and (27), respectively, using the nonlinear multiple regression tool in Origin 7.5. The value of radiative decay rate used in the fit, $\Gamma = 4.4 \times 10^7 \text{ s}^{-1}$, was calculated using the experimental $2(A)^1\Sigma^+$ potential of Ref. 68, the experimental $1(X)^1\Sigma^+$ potential of Ref. 69, and the theoretical transition dipole moment function of Ref. 70 in Le Roy's LEVEL 8.0 code.⁷¹ The 34 fitted parameters ($k_{\text{Ar}}^{\Delta J}$, $k_{\text{K}}^{\Delta J}$, $f_{\text{Ar}}^{\Delta J}$, and $f_{\text{K}}^{\Delta J}$ for each of the eight ΔJ values, and the global parameters k_{Ar}^{Q} and k_{K}^{Q}), resulting from this fit are given in Table II. Figures 6 and 7 show plots of the fluorescence and polarization data, respectively, for $\Delta J = +2$, along with the results of the global fit. Plots for other values of ΔJ are given in the supplementary material.⁶⁷ Figures 8 and 9, respectively, show plots of the collisional population transfer rate coefficients, $k_X^{\Delta J}$, and the probabilities of destruction of orientation in a collision, $f_X^{\Delta J}$, as functions of ΔJ .

B. Line-broadening measurements

Because the heat pipe oven operates at fairly high argon and potassium vapor pressures, homogeneous linewidths are dominated by collisional broadening (Doppler broadening is suppressed by the use of the OODR technique). In the course of our work, we observed the NaK $3^1\Pi(v=7, J=29) \leftarrow 2(A)^1\Sigma^+(v'=16, J'=30)$ transition lineshape at many different temperatures and pressures as we studied the transfer of population and orientation in J changing collisions. From the data, we observed that the width of this "direct" line in-

creases with both argon and potassium densities. We expect the total homogeneous linewidth, Γ_{total} , to depend on the collisional line broadening rates $k_{\text{Ar}}^{\text{Br}}n_{\text{Ar}}$ and $k_{\text{K}}^{\text{Br}}n_{\text{K}}$, the natural radiative rate Γ_{nat} , and any power broadening, Γ_{power} , that might be present according to

$$\Gamma_{\text{total}} = k_{\text{Ar}}^{\text{Br}}n_{\text{Ar}} + k_{\text{K}}^{\text{Br}}n_{\text{K}} + \Gamma_{\text{nat}} + \Gamma_{\text{power}}. \quad (29)$$

Therefore, to determine the collisional broadening (dephasing) rate coefficients we plotted the homogeneous linewidth (full width at half maximum) versus argon density at each temperature (each potassium density). These plots are linear, as expected, (an example for $n_{\text{K}} = 5.1 \times 10^{15} \text{ cm}^{-3}$ is shown in Fig. 10 and the rest of the data is presented in the online supplementary materials⁶⁷) and the slopes of the least-squares straight line fits represent the argon impact regime collisional line broadening rate coefficient, $k_{\text{Ar}}^{\text{Br}}$. Values of $k_{\text{Ar}}^{\text{Br}}$ obtained at five different potassium densities ($1.8 \times 10^{15} \text{ cm}^{-3} \leq n_{\text{K}} \leq 9.6 \times 10^{15} \text{ cm}^{-3}$) range from $(6.6 \pm 0.2) \times 10^{-9} \text{ cm}^3 \text{ s}^{-1}$ to $(7.7 \pm 0.1) \times 10^{-9} \text{ cm}^3 \text{ s}^{-1}$, with a weighted average of

$$k_{\text{Ar}}^{\text{Br}} = (7.2 \pm 0.1) \times 10^{-9} \text{ cm}^3 \text{ s}^{-1}. \quad (30)$$

The $n_{\text{Ar}} = 0$ intercepts of the plots of linewidth versus argon density represent the homogeneous broadening due to effects other than argon collisions (i.e., primarily due to potassium atom collisions). Thus the slope of a plot of these intercepts, as well as the heat pipe mode (where argon is excluded from the center of the oven) line widths, versus potassium density (see Fig. 11) yields the potassium broadening rate coefficient

$$k_{\text{K}}^{\text{Br}} = (4.5 \pm 0.2) \times 10^{-8} \text{ cm}^3 \text{ s}^{-1}. \quad (31)$$

The intercept of Fig. 11, $(3.2 \pm 0.3) \times 10^8 \text{ s}^{-1}$, represents the sum of the natural linewidth of the direct probe transition plus any power broadening that may be present.

We also observe that the collisional lines in the spectra are always substantially broader than the direct lines. Broadening of this type has been observed previously in

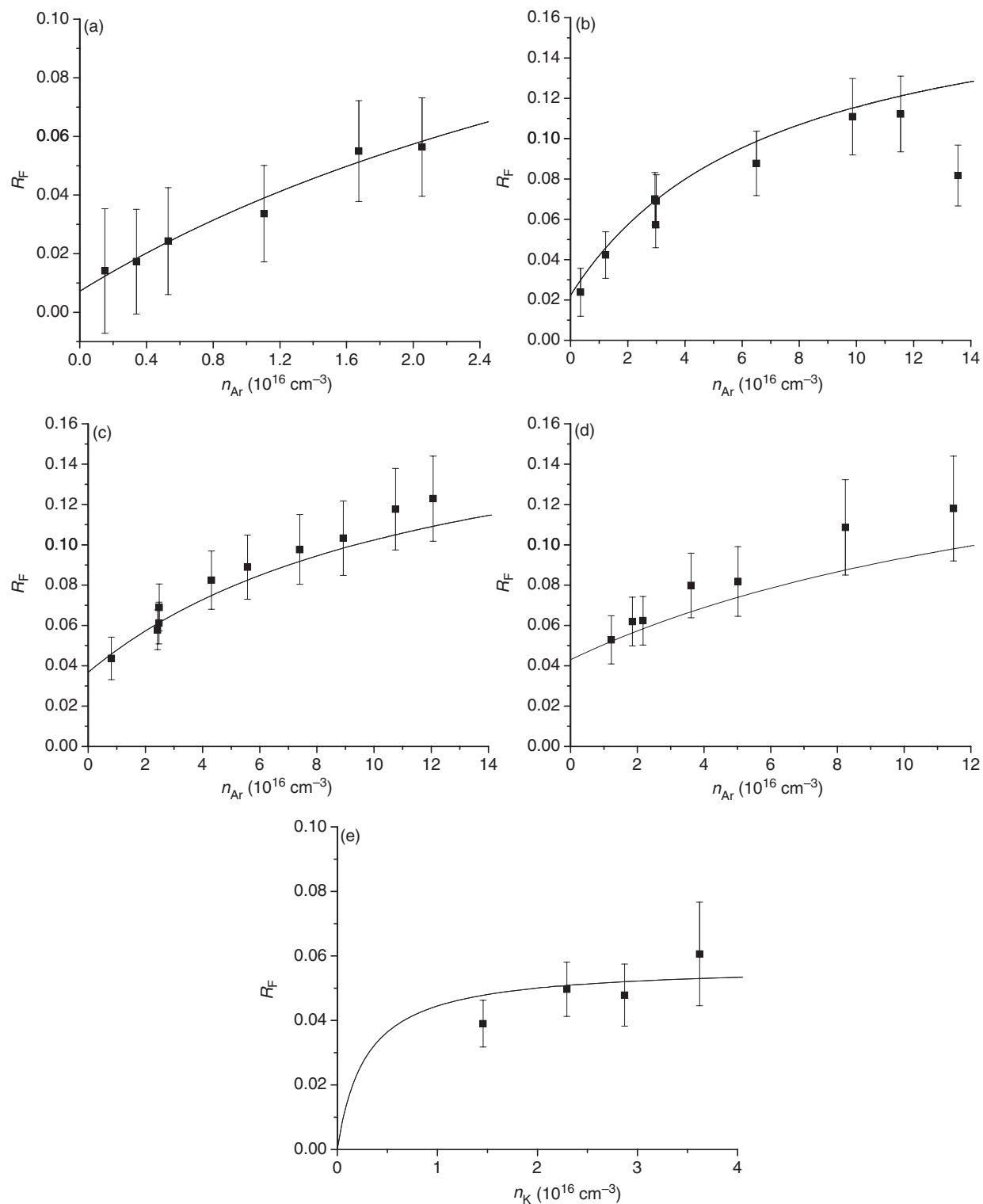


FIG. 6. Fluorescence data R_F vs n_{Ar} for $\Delta J = +2$, with the potassium density fixed at (a) $n_K = 4.1 \times 10^{14} \text{ cm}^{-3}$; (b) $n_K = 1.8 \times 10^{15} \text{ cm}^{-3}$; (c) $n_K = 5.1 \times 10^{15} \text{ cm}^{-3}$; and (d) $n_K = 8.7 \times 10^{15} \text{ cm}^{-3}$; and as a function of n_K for data obtained in the heat pipe mode (e).

rotationally inelastic collisions,^{31,52,72-76} and is due to the fact that the collisional lines correspond to molecules that have each undergone at least one rotationally inelastic collision that also causes a change in the molecule's velocity. Rotationally inelastic collisions involve much smaller impact parameters than line broadening (dephasing) collisions, and therefore the former create additional inhomogeneous broadening

since these collisions can also change the z component of the velocity of the molecule (which is initially selected to be $v_z = 0$ by the pump laser tuned to line center of the Doppler broadened pump transition). The rotationally inelastic collisional lines we observe are associated with molecules that have necessarily undergone a single strong collision (the probability that they have undergone more than one such

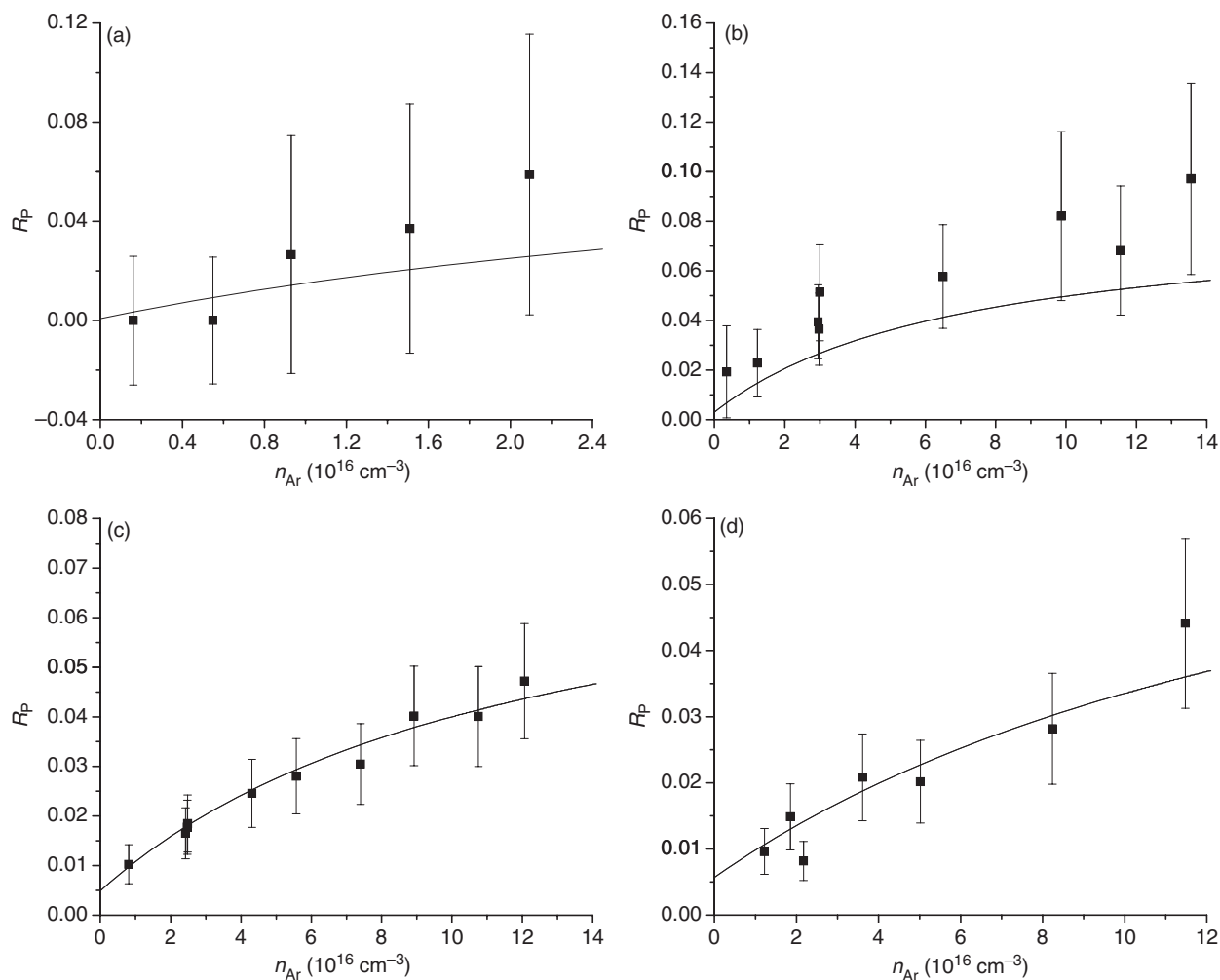


FIG. 7. Polarization data R_P vs n_{Ar} for $\Delta J = +2$, with the potassium density fixed at (a) $n_K = 3.2 \times 10^{14} \text{ cm}^{-3}$; (b) $n_K = 1.8 \times 10^{15} \text{ cm}^{-3}$; (c) $n_K = 5.1 \times 10^{15} \text{ cm}^{-3}$; and (d) $n_K = 8.7 \times 10^{15} \text{ cm}^{-3}$.

collision is less than 10%) which is also likely to change the molecule's velocity. Only a small fraction of molecules associated with direct lines are likely to have undergone such a velocity changing collision.

In a benchmark series of experiments, McCaffery and co-workers^{72–76} have demonstrated how the lineshapes of the collisional lines can be used to determine differential scattering cross sections, especially in cases where light molecules undergo collisions with heavy perturber atoms. Here we content ourselves with separating the effects of argon and potassium collisions on such velocity changes by representing the difference in linewidth of the direct line and the collisional line (Δw) as a sum of the additional broadening contributions from rotationally inelastic velocity-changing collisions with argon and potassium (Δw_{Ar} and Δw_K , respectively), weighted by the fractions of the total number of collisions in which the collision partner is an argon or potassium atom,

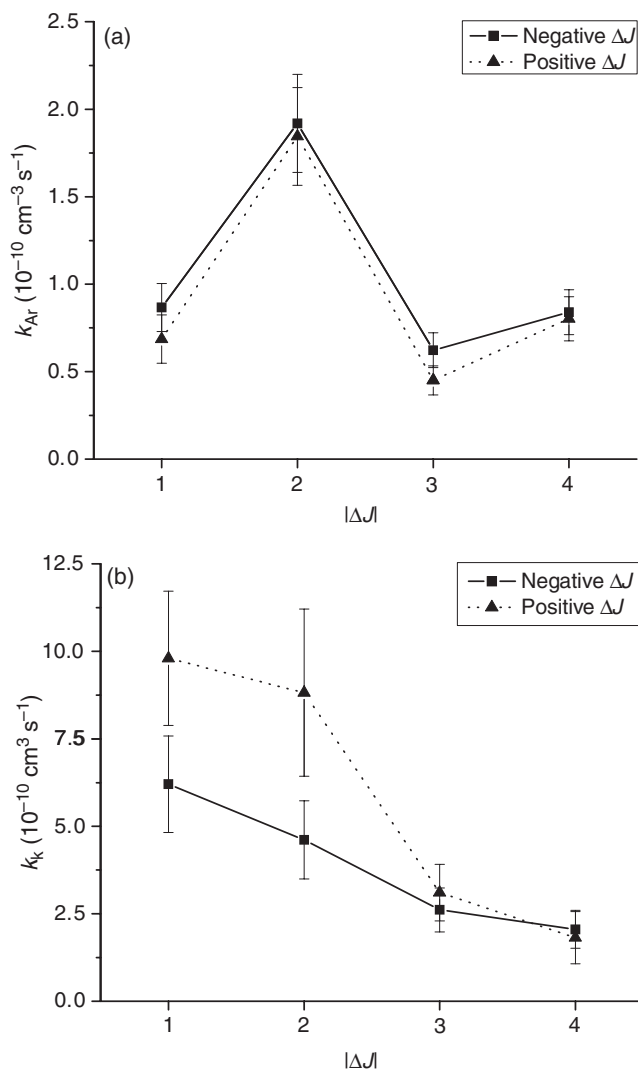
$$\Delta w = \frac{k_{Ar}^{\Delta J} n_{Ar} \Delta w_{Ar} + k_K^{\Delta J} n_K \Delta w_K}{k_{Ar}^{\Delta J} n_{Ar} + k_K^{\Delta J} n_K}. \quad (32)$$

In this simple model, we assume the homogeneous broadening of the direct and collisional transitions is the same. This is a good assumption since both transitions involve levels of the

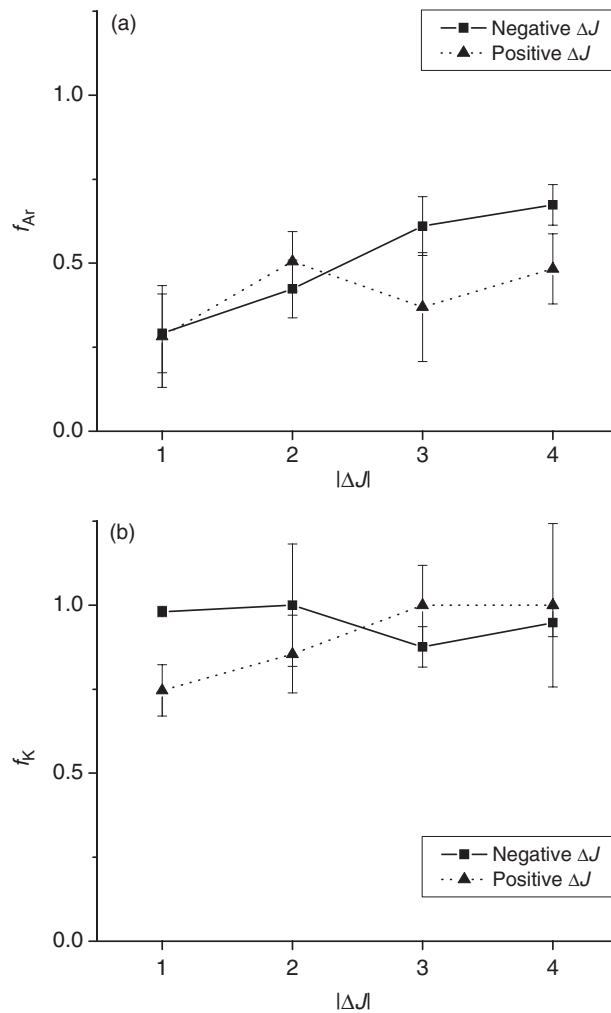
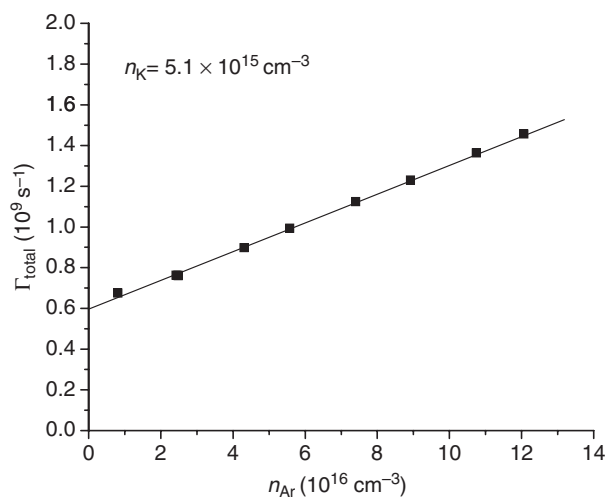
same electronic states and vibrational levels, and rotational levels differing by only one or a few units. Fitting Δw versus n_{Ar} and n_K using Eq. (32) and the known values of $k_{Ar}^{\Delta J}$ and $k_K^{\Delta J}$ we obtain values of Δw_{Ar} and Δw_K corresponding to velocity changes occurring in rotationally inelastic collisions with argon and potassium perturbers and for each ΔJ . These values are shown in Fig. 12.

C. Assignment of uncertainties

The major sources of uncertainty in our measured population transfer rate coefficients, probabilities for destruction of orientation in rotationally inelastic collisions, and line broadening rate coefficients are the uncertainties in the determination of the potassium and argon densities. The uncertainty in the potassium density is particularly large because the heat pipe oven is far from an ideal environment for determining atomic densities. Certainly, the heat pipe oven environment is not in thermal equilibrium. Standard alkali vapor cells provide uniform densities and are therefore generally preferable for collision studies, but they cannot be operated at the elevated temperatures necessary to produce sufficiently high molecular densities.

FIG. 8. Fitted values of (a) $k_{\text{Ar}}^{\Delta J}$ and (b) $k_{\text{K}}^{\Delta J}$ plotted against ΔJ .

In this work, we initially determined the potassium density from the Nesmeyanov vapor pressure formula. However, in addition to the problems mentioned above, and although we have multiple thermocouple sensors on the heat pipe, we do not necessarily measure the highest temperature where the liquid metal sits (which controls the actual vapor pressure), and the Nesmeyanov formula itself may have a systematic error in the pressure range used in this work. Finally, the presence of sodium in the alkali mixture is likely to reduce the potassium density in the vapor phase, according to the basic mechanism of Raoult's law.⁷⁷ This last effect would be partially compensated by the presence of some sodium vapor which is likely to act similarly to potassium in these collision processes. In order to obtain an independent check on the potassium densities and to assign reasonable values to their uncertainties, we carried out measurements of the potassium D1 and D2 line ($4S_{1/2} \rightarrow 4P_{1/2}$ and $4S_{1/2} \rightarrow 4P_{3/2}$ transitions, respectively) absorption equivalent widths⁷⁸ using the white light and monochromator shown in Fig. 2 and of the D2 line blue wing absorption coefficient using the cw dye laser, when the oven was operated in both heat pipe mode and oven mode.

FIG. 9. Fitted values of (a) $f_{\text{Ar}}^{\Delta J}$ and (b) $f_{\text{K}}^{\Delta J}$ plotted against ΔJ .FIG. 10. Plot of the homogeneous linewidths of the "direct" probe transition, $3^1\Pi(v=7, J=29) \leftarrow 2(A)^1\Sigma^+(v'=16, J'=30)$, as a function of argon density, for $n_{\text{K}} = 5.1 \times 10^{15} \text{ cm}^{-3}$. The slope of the least-squares straight line fit of these data is $(7.05 \pm 0.11) \times 10^{-9} \text{ cm}^3 \text{ s}^{-1}$ and the intercept is $(5.96 \pm 0.08) \times 10^8 \text{ s}^{-1}$.

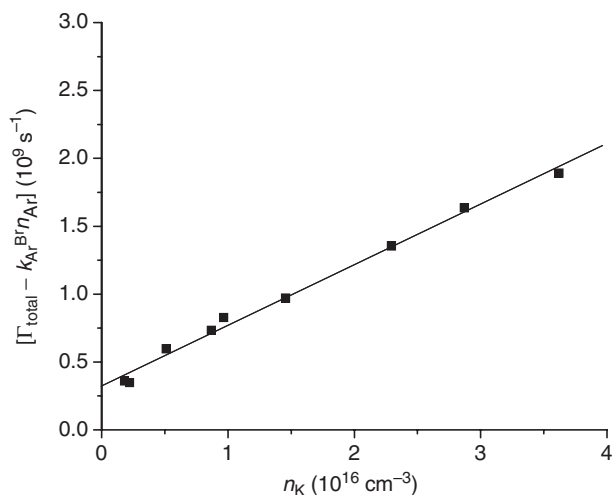


FIG. 11. $n_{\text{Ar}} = 0$ intercepts of the homogeneous linewidths vs argon density of the “direct” probe transition, $3^1\Pi(v = 7, J = 29) \leftarrow 2(A)^1\Sigma^+(v' = 16, J' = 30)$, plus linewidths recorded in heat pipe mode, plotted as a function of potassium density. The slope of the least-squares straight line fit of these data is $k_{\text{K}}^{\text{Br}} = (4.5 \pm 0.2) \times 10^{-8} \text{ cm}^3 \text{ s}^{-1}$ with an intercept of $(3.2 \pm 0.3) \times 10^8 \text{ s}^{-1}$.

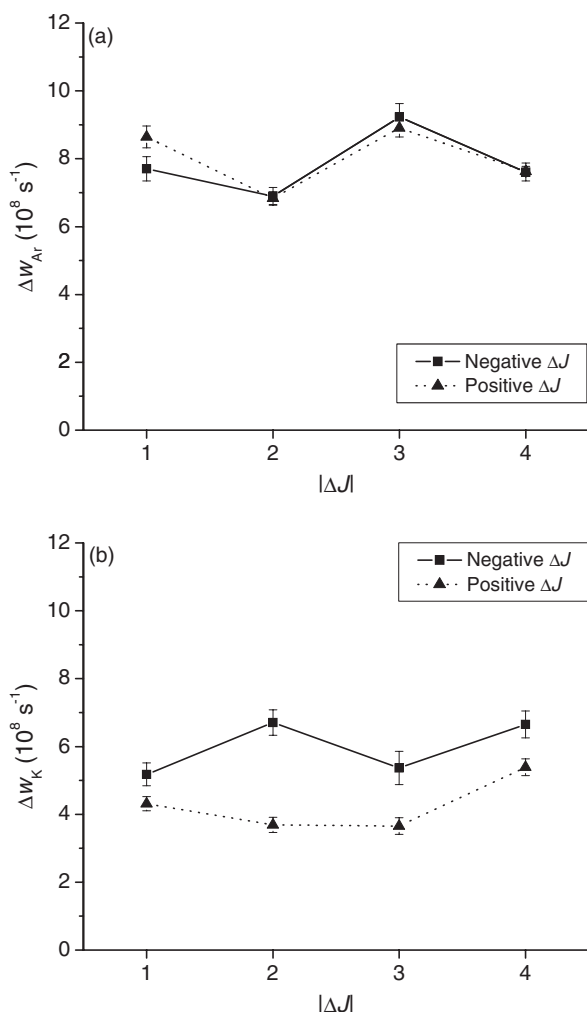


FIG. 12. Velocity changes (as manifested in additional Doppler broadening of collisional lines) due to (a) argon collisions and (b) potassium collisions.

The latter method has been described in detail by Horvatic *et al.*⁷⁹ To determine the equivalent width, we calculated the absorption coefficient as a function of detuning around the D1 and D2 lines including the effects of Doppler broadening, collisional broadening due to potassium perturbers (using the self-broadening rates of Carrington *et al.*⁸⁰), collisional broadening due to argon perturbers when operating in oven mode (using the argon broadening rates of Lwin *et al.*^{81,82}), and hyperfine structure (using the hyperfine constants reported in Ref. 83). Potassium densities were adjusted until the calculated absorption equivalent widths matched the experimental values. Potassium densities measured using the equivalent width method were lower than those obtained from the Nesmeyanov formula by amounts ranging from 3% to 33% with an average of 20.2%. We also determined potassium densities by comparing the measured D2 line blue wing absorption coefficient at specific detunings with absorption coefficients calculated as described above and, in the case where we operated the oven in heat-pipe mode (where the argon is excluded from the central region), calculated using the effective C_3 coefficient and more realistic lineshape provided by Horvatic *et al.*⁷⁹ Densities obtained by comparing measured D2 line blue wing absorption obtained in heat pipe mode to values calculated using the Carrington *et al.* self-broadening rates were lower than those calculated from the Nesmeyanov formula by 15%–25% (with an average of 20.6%). Similarly densities obtained by comparing measured wing absorption obtained in oven mode to values calculated using the Carrington *et al.* self-broadening rates and the Lwin *et al.* argon broadening rates were lower than those calculated from the Nesmeyanov formula by 10%–28% (with an average of 19.9%). Finally, densities obtained by comparing measured wing absorption obtained in heat pipe mode to values calculated using the effective C_3 coefficient of Horvatic *et al.* were lower than those calculated from the Nesmeyanov formula by 23%–32% (with an average of 27.3%). Thus our measurements and analysis indicate that the Nesmeyanov formula systematically overestimates the potassium densities by an average of 22% in this situation where potassium and sodium metals are heated together, in agreement with the basic prediction of Raoult’s law. Therefore in our analysis, we used potassium densities given by the Nesmeyanov formula, but corrected downward by 22%, and we assign 30% uncertainties to these corrected densities. These uncertainties, which we believe to be quite conservative, are consistent with previous studies in our laboratory.^{84,85} In addition, we do not consider the neglect of the Na, K₂, NaK, and Na₂ densities to be a serious limitation since the sodium atomic density is less than 10%, and the molecular densities are all less than 1%, of the potassium density.

When operating in oven mode, we determine the argon partial pressure by subtracting the calculated potassium partial pressure (obtained from the Nesmeyanov formula with the correction discussed above) from the total pressure measured in the heat pipe using the capacitance manometer. The manometer has a precision of 0.1 Torr, and as stated above we assign a 30% uncertainty to the potassium density or pressure. Thus we calculate the fractional uncertainty in the argon pressure (and density) using the

formula,

$$\frac{\Delta P_{\text{Ar}}}{P_{\text{Ar}}} = \frac{0.1 \text{ Torr}}{P_{\text{Ar}}} + 0.3 \frac{P_{\text{K}}}{P_{\text{Ar}}}. \quad (33)$$

Here the first term on the right-hand side represents the uncertainty due to the pressure gauge, and the second term represents the fractional uncertainty contribution from the potassium partial pressure.

The uncertainties in the potassium and argon densities are incorporated into the dependent variable of the fitted empirical models for the fluorescence and polarization spectroscopy intensity ratios using

$$\Delta R_{\text{F}} = \left| \frac{dR_{\text{F}}}{dn_{\text{Ar}}} \right| \Delta n_{\text{Ar}} + \left| \frac{dR_{\text{F}}}{dn_{\text{K}}} \right| \Delta n_{\text{K}}. \quad (34)$$

From Eq. (17), we obtain

$$\left| \frac{dR_{\text{F}}/dn_{\text{Ar}}}{R_{\text{F}}} \right| = \left| \frac{\frac{k_{\text{Ar}}^{\Delta J}}{\Gamma}}{\frac{k_{\text{Ar}}^{\Delta J}}{\Gamma} n_{\text{Ar}} + \frac{k_{\text{K}}^{\Delta J}}{\Gamma} n_{\text{K}}} - \frac{\frac{k_{\text{Ar}}^{\text{Q}}}{\Gamma}}{1 + \frac{k_{\text{Ar}}^{\text{Q}}}{\Gamma} n_{\text{Ar}} + \frac{k_{\text{K}}^{\text{Q}}}{\Gamma} n_{\text{K}}} \right| \quad (35)$$

and

$$\left| \frac{dR_{\text{F}}/dn_{\text{K}}}{R_{\text{F}}} \right| = \left| \frac{\frac{k_{\text{K}}^{\Delta J}}{\Gamma}}{\frac{k_{\text{Ar}}^{\Delta J}}{\Gamma} n_{\text{Ar}} + \frac{k_{\text{K}}^{\Delta J}}{\Gamma} n_{\text{K}}} - \frac{\frac{k_{\text{K}}^{\text{Q}}}{\Gamma}}{1 + \frac{k_{\text{Ar}}^{\text{Q}}}{\Gamma} n_{\text{Ar}} + \frac{k_{\text{K}}^{\text{Q}}}{\Gamma} n_{\text{K}}} \right|. \quad (36)$$

Preliminary estimates for the $k_{\text{X}}^{\Delta J}$ and k_{X}^{Q} parameters were used to evaluate these contributions to the uncertainties in R_{F} . The equations for the uncertainty contributions in the polarization spectroscopy model are of a similar form; one needs only to replace R_{F} by R_{P} , and $k_{\text{X}}^{\Delta J}$ and k_{X}^{Q} by $k_{\text{X}}^{\text{O},\Delta J}$ and g_{X} , respectively. These contributions are added to the statistical uncertainties due to fluctuations in intensity to obtain the total uncertainty in each intensity ratio used in the fit. These total uncertainties in the R_{F} and R_{P} values are listed in the supplementary material's Tables 1 and 2.⁶⁷

The weighted R_{F} and R_{P} values are fitted with expressions (17) and (27) using the nonlinear multiple regression tool of Origin 7.5.

Finally, the use of rate equation models [Eqs. (17) and (27)] to analyze the collisional to direct line intensity ratios in the fluorescence and polarization spectroscopy experiments may also contribute to error in our results, since rate equation models neglect laser-induced coherences. One can show⁸⁶ that the steady state density matrix equations of motion reduce to rate equations when no level interacts with more than one laser field (as, for example, in the case where we probe the collisionally populated intermediate state levels). However, for the direct lines, where both pump and probe lasers interact with the same intermediate state level, coherences can be important. Therefore, we have developed a full density matrix treatment of the direct line intensities, in both fluorescence and polarization spectroscopy, to examine these effects. Using this model, we have

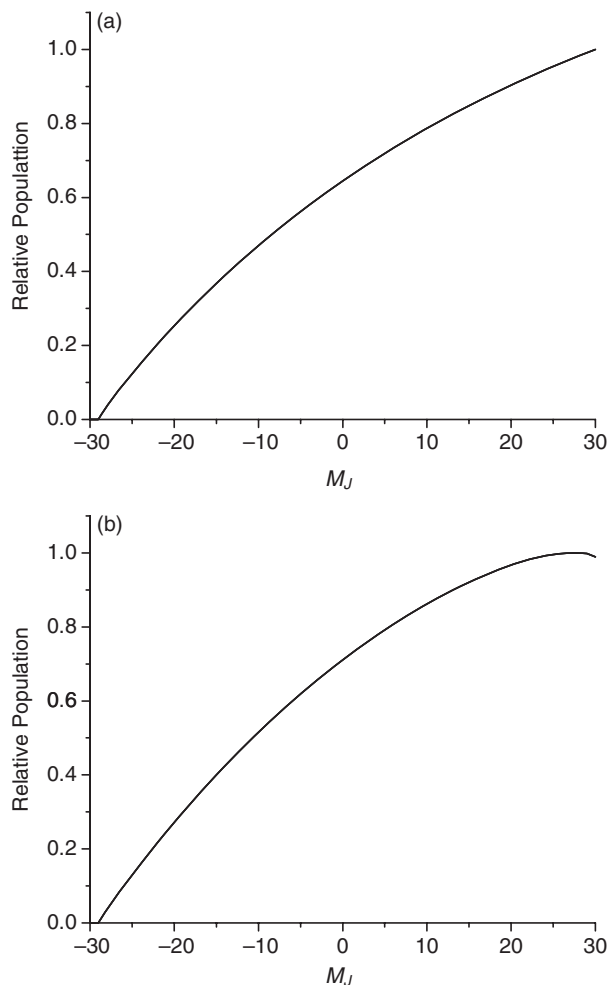


FIG. 13. M_J level population distribution in the intermediate $2(A)^1\Sigma^+(v' = 16, J' = 30)$ level calculated using the density matrix equations of motion for the NaK OODR transition $3^1\Pi(v = 7, J = 29) \leftarrow 2(A)^1\Sigma^+(v' = 16, J' = 30) \leftarrow 1(X)^1\Sigma^+(v'' = 0, J'' = 29)$. (a) Pump laser power 100 mW, probe laser power 0 mW. Net orientation $\langle M_J \rangle = 8.62$. (b) Pump laser power 100 mW, probe laser power 1 mW. Net orientation $\langle M_J \rangle = 8.38$. The conditions of case (b) are similar to those used in the present experiment.

determined that a 1 mW probe laser with 1 mm beam radius at the cell (similar to the conditions used in this experiment) changes the intermediate state population by less than 6% and orientation by less than 3% compared to the case with no probe laser (see Fig. 13).⁸⁶ We believe this sets an upper limit on the uncertainty introduced by using a rate equation model in the analysis. A more complete description of the density matrix equations of motion can be found in Ref. 86. Analysis of the polarization lineshapes using the density matrix equations is ongoing.

V. CONCLUSIONS

Our data show that there is a strong propensity for collisions of argon atoms with NaK molecules to change J by an even number. This propensity has been observed previously for collisions involving other heteronuclear molecules⁸⁷⁻⁹⁰ and is due to interference effects when the anisotropy of the interaction potential energy surface for the atom-molecule

collision is not very large.^{91,92} In such a case, the molecule can be considered to be “almost homonuclear.”⁹¹ For example, Antonova *et al.*⁹⁰ found a very strong $\Delta J = \text{even}$ propensity in the almost homonuclear ${}^6\text{Li}{}^7\text{Li}$ molecule. As is well known, homonuclear molecules in ${}^1\Sigma$ states have a strict $\Delta J = \pm 2, \pm 4, \text{etc.}$, selection rule for collisional spectra due to nuclear symmetry arguments. In contrast to the present results for NaK, and the earlier work on ${}^6\text{Li}{}^7\text{Li}$,⁹⁰ preliminary work in our laboratory on collisions of NaCs molecules with argon atoms shows no such propensity.⁹³ This follows from the argument that NaCs is “more heteronuclear” implying that the anisotropies in the potential energy surface are more significant. However, both McCurdy and Miller⁹¹ and Maricq⁹² point out that the situation is more complicated than this simple view, with calculations showing propensities for $\Delta J = \text{odd}$ transitions for certain choices of the anisotropy parameters (coefficients of the even and odd Legendre polynomial terms used to describe the interaction potential).⁹¹ We also note that McCormack and McCaffery²⁵ found a $\Delta J = \text{even}$ propensity for the transfer of orientation (but not for transfer of population) for collisions of He atoms with NaK molecules in ${}^1\Pi$ states.

The propensity toward even-numbered changes in J is not seen in collisions of NaK with potassium, although the data do show that, in this case, positive ΔJ is favored over negative ΔJ . An asymmetry with respect to the sign of $\Delta J = \text{odd}$ transitions has been observed before in Refs. 3–7 for collisions of homonuclear alkali molecules in ${}^1\Pi_u$ levels with noble gas atoms, where it was attributed to different atom–molecule potential surfaces associated with the two lambda doubling components. An asymmetry in positive versus negative ΔJ collisions in the $\text{Li}_2 A^1\Sigma_u^+$ –noble gas system was also shown in Ref. 28. In contrast, our analysis of collisions involving NaK $A^1\Sigma^+$ molecules, where we separate the effects of argon and potassium collisions, shows an asymmetry with respect to the sign of ΔJ in the population transfer rate coefficients for collisions with potassium atoms, but not for collisions with argon atoms.

We have also observed that collisions of NaK molecules with potassium atoms are more likely to transfer population to neighboring rotational levels than collisions with argon atoms ($k_{\text{Ar}}^{\Delta J} < k_{\text{K}}^{\Delta J}$ for all ΔJ) and that the probability of destroying orientation in such rotationally inelastic collisions is also much larger for potassium than for argon perturbers. According to our analysis, the fraction of the initial orientation that is destroyed in a rotationally inelastic collision with a potassium atom is characterized by $f_{\text{K}}^{\Delta J} \sim 1$, meaning that virtually all of the initial angular momentum orientation is lost in a single rotationally inelastic collision. In contrast, $0.28 < f_{\text{Ar}}^{\Delta J} < 0.67$, indicating that rotationally inelastic collisions with argon atoms tend to preserve a substantial fraction of the initial orientation. [We note our values of $(1 - f_{\text{Ar}}^{\Delta J})$ are of about the same magnitude as the equivalent σ^1/σ^0 parameters determined for rotationally inelastic collisions of NaK(${}^1\Pi$) molecules with helium atoms by McCormack and McCaffery,²⁵ who measured the circular polarization and total intensity of fluorescence emitted by directly excited molecules and those in collisionally populated levels.] Presumably a collision of a potassium atom with an

NaK molecule is more likely to affect either the magnitude, J , or the direction, M_J , of the molecular angular momentum than does a collision with an argon atom, due to the nonzero angular momentum of the potassium atom’s loosely bound outer valence electron.

We note that most of the fitted parameters in our rate equation models are of the form k/Γ , which were converted to rate coefficients using the value $\Gamma = 4.4 \times 10^7 \text{ s}^{-1}$ for the NaK $2(A)^1\Sigma^+(v' = 16, J')$ level radiative rate. This value of Γ was calculated using Le Roy’s LEVEL 8.0 code⁷¹ with the $2(A)^1\Sigma^+$ potential of Ref. 68, the $1(X)^1\Sigma^+$ potential of Ref. 69, and the $2(A)^1\Sigma^+ \leftrightarrow 1(X)^1\Sigma^+$ transition dipole moment of Ref. 70. However, if an improved value for Γ is found in the future, our results can easily be corrected to take this into account.

Regarding the line broadening measurements, we see that the rate coefficient for broadening of NaK transitions by potassium perturbers is approximately six times larger than that for argon. We believe this is due to the fact that the potassium atom is much more polarizable than argon. Our value for the broadening rate coefficient of the NaK $3^1\Pi(v = 7, J = 29) \leftarrow 2(A)^1\Sigma^+(v' = 16, J' = 30)$ line due to collisions with argon is 2–8 times larger than values for alkali resonance lines broadened by argon.^{81,82} In addition, the broadening rate we have obtained for the NaK $3^1\Pi(v = 7, J = 29) \leftarrow 2(A)^1\Sigma^+(v' = 16, J' = 30)$ line broadened by collisions with potassium atoms is also ~6–8 times greater than those obtained previously by Kamke *et al.*⁹⁴ for broadening of the sodium resonance lines by collisions with dissimilar alkali (rubidium and cesium) atoms. We believe that these differences may be due to the permanent dipole moment and larger polarizability of the molecule. The broadening rates measured here are also useful for solving the density matrix equations of motion, since the line-broadening rate is equal to twice the collisional dephasing rate needed in these calculations.

Finally, from the results of Fig. 12, we observe that the velocity changes in rotationally inelastic collisions are larger for argon than for potassium perturbers. We believe that this is because the rate coefficient for argon J -changing collisions is smaller than that for potassium, and therefore J -changing collisions of NaK molecules with argon atoms must have smaller impact parameters than J -changing collisions with potassium. Thus the argon J -changing collision perturbs the translational motion of the molecule more than a similar collision with potassium. In the present work, we do not observe much increase in linewidth with increasing ΔJ . This is in contrast to McCaffery and co-workers^{72–76} who observed a significant increase, with increasing ΔJ , in the broadening due to velocity changes in Li_2 –Xe rotationally inelastic collisions. McCaffery also observed significant differences in the broadening of lines with positive versus negative ΔJ , whereas we see almost no difference for argon collisions but some difference for potassium collisions (see Fig. 12). We believe the difference between these observations can be attributed to the different molecule/atom mass ratio in the two experiments. The lineshape measurements of Kasahara *et al.*³¹ on NaK $G^1\Delta(v = 15, J = 29 + \Delta J) \leftarrow B^1\Pi(v' = 9, J' = 30 + \Delta J)$ transitions following rotationally inelastic

collisions with argon were carried to larger ΔJ than studied here, and show a clear trend of increasing linewidth with increasing ΔJ (even in the region $1 \leq |\Delta J| \leq 4$ corresponding to the present work). But as in the present work, they did not observe much asymmetry with the sign of ΔJ , and the magnitude of the broadening measured in Ref. 31 is also consistent with the values reported here. A more detailed comparison is not possible because the role of the argon versus potassium atom collisions was not distinguished in Ref. 31. Last, we note that the work of Kasahara *et al.*³¹ also presents a very interesting study of linewidths associated with ground state collisions, showing polarization spectroscopy linewidths out to $\Delta J = 50$.

ACKNOWLEDGMENTS

We would like to thank Dr. Amanda Ross, Professor Robert W. Field and Professor A. Peet Hickman for many valuable discussions. This work was supported by the National Science Foundation through Grant Nos. PHY-0652938, PHY-0968898, PHY-0555608, and PHY-0855502.

- ¹H. Salami, T. Bergeman, B. Beser, J. Bai, E. H. Ahmed, S. Kotochigova, A. M. Lyyra, J. Huennekens, C. Lisdat, A. V. Stolyarov, O. Dulieu, P. Crozet, and A. J. Ross, *Phys. Rev. A* **80**, 022515 (2009).
- ²J. Bai, E. H. Ahmed, B. Beser, Y. Guan, S. Kotochigova, A. M. Lyyra, S. Ashman, C. M. Wolfe, J. Huennekens, F. Xie, D. Li, L. Li, M. Tamanis, R. Ferber, A. Drozdova, E. Pazyuk, A. V. Stolyarov, J. G. Danzl, H.-C. Nägerl, N. Bouloufa, O. Dulieu, C. Amiot, H. Salami, and T. Bergeman, *Phys. Rev. A* **83**, 032514 (2011).
- ³K. Bergmann and W. Demtröder, *Z. Phys.* **243**, 1 (1971).
- ⁴K. Bergmann and W. Demtröder, *J. Phys. B* **5**, 1386 (1972).
- ⁵K. Bergmann and W. Demtröder, *J. Phys. B* **5**, 2098 (1972).
- ⁶Ch. Ottinger, R. Velasco, and R. N. Zare, *J. Chem. Phys.* **52**, 1636 (1970).
- ⁷Ch. Ottinger and D. Poppe, *Chem. Phys. Lett.* **8**, 513 (1971).
- ⁸T. A. Brunner, R. D. Driver, N. Smith, and D. E. Pritchard, *J. Chem. Phys.* **70**, 4155 (1979).
- ⁹T. P. Scott, N. Smith, and D. E. Pritchard, *J. Chem. Phys.* **80**, 4841 (1984).
- ¹⁰B. Stewart, P. D. Magill, T. P. Scott, J. Derouard, and D. E. Pritchard, *Phys. Rev. Lett.* **60**, 282 (1988).
- ¹¹P. D. Magill, B. Stewart, N. Smith, and D. E. Pritchard, *Phys. Rev. Lett.* **60**, 1943 (1988).
- ¹²P. D. Magill, T. P. Scott, N. Smith, and D. E. Pritchard, *J. Chem. Phys.* **90**, 7195 (1989).
- ¹³B. Stewart, P. D. Magill, and D. E. Pritchard, *J. Phys. Chem. A* **104**, 10565 (2000).
- ¹⁴A. J. McCaffery, *J. Chem. Phys.* **111**, 7697 (1999).
- ¹⁵S. Coppage, P. Matei, and B. Stewart, *J. Chem. Phys.* **128**, 241103 (2008).
- ¹⁶Y. Gao and B. Stewart, *J. Chem. Phys.* **103**, 860 (1995).
- ¹⁷Y. Gao, P. S. Gorgone, S. Davis, E. K. McCall, and B. Stewart, *J. Chem. Phys.* **104**, 1415 (1996).
- ¹⁸M. H. Alexander and H.-J. Werner, *J. Chem. Phys.* **95**, 6524 (1991).
- ¹⁹J. C. Flasher and R. C. Forrey, *Phys. Rev. A* **65**, 032710 (2002).
- ²⁰P. M. Florian, M. Hoster, and R. C. Forrey, *Phys. Rev. A* **70**, 032709 (2004).
- ²¹G. Quéméner, N. Balakrishnan, and R. V. Krems, *Phys. Rev. A* **77**, 030704 (2008).
- ²²N. Balakrishnan, B. C. Hubartt, L. Ohlinger, and R. C. Forrey, *Phys. Rev. A* **80**, 012704 (2009).
- ²³R. Teets, R. Feinberg, T. W. Hänsch, and A. L. Schawlow, *Phys. Rev. Lett.* **37**, 683 (1976).
- ²⁴M. D. Rowe and A. J. McCaffery, *Chem. Phys.* **43**, 35 (1979).
- ²⁵J. McCormack and A. J. McCaffery, *Chem. Phys.* **51**, 405 (1980).
- ²⁶M. H. Alexander and S. L. Davis, *J. Chem. Phys.* **78**, 6754 (1983).
- ²⁷J. Derouard, *Chem. Phys.* **84**, 181 (1984).
- ²⁸C. Ottinger and M. Schroder, *J. Phys. B* **13**, 4163 (1980).
- ²⁹K. T. Lorenz, D. W. Chandler, J. W. Barr, W. Chen, G. L. Barnes, and J. I. Cline, *Science* **293**, 2063 (2001).
- ³⁰J. I. Cline, K. T. Lorenz, E. A. Wade, J. W. Barr, and D. W. Chandler, *J. Chem. Phys.* **115**, 6277 (2001).
- ³¹S. Kasahara, H. Ikoma, and H. Katô, *Acta Phys. Hung.* **74**, 329 (1994).
- ³²R. J. Wilson and A. J. McCaffery, *Chem. Phys. Lett.* **261**, 195 (1996).
- ³³A. J. McCaffery and R. J. Wilson, *J. Phys. B* **30**, 5773 (1997).
- ³⁴H. J. Crichton, M. L. Costen, and K. G. McKendrick, *J. Chem. Phys.* **119**, 9461 (2003).
- ³⁵M. L. Costen, H. J. Crichton, and K. G. McKendrick, *J. Chem. Phys.* **120**, 7910 (2004).
- ³⁶M. L. Costen and K. G. McKendrick, *J. Chem. Phys.* **122**, 164309 (2005).
- ³⁷S. Marinakis, G. Paterson, J. Klos, M. L. Costen, and K. G. McKendrick, *Phys. Chem. Chem. Phys.* **9**, 4414 (2007).
- ³⁸S. Marinakis, G. Paterson, G. Richmond, M. Rockingham, M. L. Costen, and K. G. McKendrick, *J. Chem. Phys.* **128**, 021101 (2008).
- ³⁹G. Paterson, S. Marinakis, M. L. Costen, K. G. McKendrick, J. Klos, and R. Toboła, *J. Chem. Phys.* **129**, 074304 (2008).
- ⁴⁰M. Brouard, A. Bryant, I. Burak, S. Marinakis, F. Quadriani, I. Anton Garcia, and C. Vallance, *Mol. Phys.* **103**, 1693 (2005).
- ⁴¹M. Brouard, A. Bryant, Y.-P. Chang, R. Cireasa, C. J. Eyles, A. M. Green, S. Marinakis, F. J. Aoiz, and J. Klos, *J. Chem. Phys.* **130**, 044306 (2009).
- ⁴²M. L. Costen, R. Livingstone, K. G. McKendrick, G. Paterson, M. Brouard, H. Chadwick, Y.-P. Chang, C. J. Eyles, F. J. Aoiz, and J. Klos, *J. Phys. Chem. A* **113**, 15156 (2009).
- ⁴³Jianmei Bai, Ph.D. dissertation, Temple University, 2011 (unpublished).
- ⁴⁴C. R. Vidal and J. Cooper, *Appl. Phys.* **40**, 3370 (1969).
- ⁴⁵N. W. Carlson, F. V. Kowalski, R. E. Teets, and A. L. Schawlow, *Opt. Commun.* **29**, 302 (1979).
- ⁴⁶R. A. Bernheim, L. P. Gold, and T. Tipton, *J. Chem. Phys.* **78**, 3635 (1983).
- ⁴⁷H. Wang, L. Li, A. M. Lyyra, and W. C. Stwalley, *J. Mol. Spectrosc.* **137**, 304 (1989).
- ⁴⁸C.-C. Tsai, J. T. Bahns, T.-J. Whang, H. Wang, W. C. Stwalley, and A. M. Lyyra, *Phys. Rev. Lett.* **71**, 1152 (1993).
- ⁴⁹J. T. Kim, C. C. Tsai, and W. C. Stwalley, *J. Mol. Spectrosc.* **171**, 200 (1995).
- ⁵⁰N. Okada, S. Kasahara, T. Ebi, M. Baba, and H. Katô, *J. Chem. Phys.* **105**, 3458 (1996).
- ⁵¹G. Zhao, J. T. Kim, J. T. Bahns, and W. C. Stwalley, *J. Mol. Spectrosc.* **184**, 209 (1997).
- ⁵²Z. J. Jabbour and J. Huennekens, *J. Chem. Phys.* **107**, 1094 (1997).
- ⁵³A. Pashov, I. Jackowska, W. Jastrzębski, and P. Kowalczyk, *Phys. Rev. A* **58**, 1048 (1998).
- ⁵⁴S. Kasahara, C. Fujiwara, N. Okada, H. Katô, and M. Baba, *J. Chem. Phys.* **111**, 8857 (1999).
- ⁵⁵E. Laub, I. Mazza, S. C. Webb, J. LaCivita, I. Prodan, Z. J. Jabbour, R. K. Namiotka, and J. Huennekens, *J. Mol. Spectrosc.* **193**, 376 (1999); Erratum, *J. Mol. Spectrosc.* **221**, 142 (2003).
- ⁵⁶S. Kasahara, P. Kowalczyk, M. H. Kabir, M. Baba, and H. Katô, *J. Chem. Phys.* **113**, 6227 (2000).
- ⁵⁷P. O'Keeffe, T. Ridley, K. P. Lawley, R. J. Donovan, H. H. Telle, D. C. S. Beddows, and A. G. Urena, *J. Chem. Phys.* **113**, 2182 (2000).
- ⁵⁸S. Antonova, G. Lazarov, K. Urbanski, A. M. Lyyra, Li Li, G.-H. Jeung, and W. C. Stwalley, *J. Chem. Phys.* **112**, 7080 (2000).
- ⁵⁹E. Kagi, N. Yamamoto, H. Fujiwara, M. Fukushima, and T. Ishiwata, *J. Mol. Spectrosc.* **216**, 48 (2002).
- ⁶⁰N. Bouloufa, L. Cabaret, P. Luc, R. Vetter, and W. T. Luh, *J. Chem. Phys.* **121**, 7237 (2004).
- ⁶¹M. Braune, H. Valipour, and D. Zimmermann, *J. Mol. Spectrosc.* **235**, 84 (2006).
- ⁶²J. Ye, H. F. Pang, and A. S.-C. Cheung, *Chem. Phys. Lett.* **442**, 251 (2007).
- ⁶³A. N. Nesmeyanov, *Vapor Pressure of the Elements* (Academic, New York, 1963).
- ⁶⁴C. Wieman and T. W. Hänsch, *Phys. Rev. Lett.* **36**, 1170 (1976).
- ⁶⁵W. Demtröder, *Laser Spectroscopy, Volume 2 Experimental Techniques*, 4th ed. (Springer-Verlag, Berlin, 2008).
- ⁶⁶F. C. Spano, *J. Chem. Phys.* **114**, 276 (2001).
- ⁶⁷See supplementary material at <http://dx.doi.org/10.1063/1.3575234> for complete data tables and figures.
- ⁶⁸A. J. Ross, R. M. Clements, and R. F. Barrow, *J. Mol. Spectrosc.* **127**, 546 (1988).
- ⁶⁹I. Russier-Antoine, A. J. Ross, M. Aubert-Frécon, F. Martin, and P. Crozet, *J. Phys. B* **33**, 2753 (2000).
- ⁷⁰S. Magnier, M. Aubert-Frécon, and Ph. Millié, *J. Mol. Spectrosc.* **200**, 96 (2000).

- ⁷¹R. J. Le Roy, "LEVEL 8.0: A computer program for solving the radial Schrodinger equation for bound and quasibound levels," *University of Waterloo Physics Research Report CP-663*, 2007. See <http://leroy.uwaterloo.ca/programs/>.
- ⁷²A. J. McCaffery, K. L. Reid, and B. J. Whitaker, *Phys. Rev. Lett.* **61**, 2085 (1988).
- ⁷³K. L. Reid and A. J. McCaffery, *J. Chem. Phys.* **96**, 5789 (1992).
- ⁷⁴A. J. McCaffery, J. P. Richardson, R. J. Wilson, and M. J. Wynn, *J. Phys. B* **26**, L705 (1993).
- ⁷⁵T. L. D. Collins, A. J. McCaffery, J. P. Richardson, and M. J. Wynn, *Phys. Rev. Lett.* **70**, 3392 (1993).
- ⁷⁶T. L. D. Collins, A. J. McCaffery, J. P. Richardson, R. J. Wilson, and M. J. Wynn, *J. Chem. Phys.* **102**, 4419 (1995).
- ⁷⁷R. Chang, *General Chemistry* (McGraw-Hill Higher Education, New York, 2000), pp. 415–416.
- ⁷⁸A. Corney, *Atomic and Laser Spectroscopy* (Clarendon, Oxford, 1977).
- ⁷⁹V. Horvatic, M. Movre, R. Beuc, and C. Vadla, *J. Phys. B* **26**, 3679 (1993).
- ⁸⁰C. G. Carrington, D. N. Stacey, and J. Cooper, *J. Phys. B* **6**, 417 (1973).
- ⁸¹N. Lwin, D. G. McCartan, and E. L. Lewis, *Astrophys. J.* **213**, 599 (1977).
- ⁸²E. L. Lewis, *Phys. Rep.* **58**, 1 (1980).
- ⁸³E. Arimondo, M. Inguscio, and P. Violino, *Rev. Mod. Phys.* **49**, 31 (1977).
- ⁸⁴Z. J. Jabbour, J. Sagle, R. K. Namiotka, and J. Huennekens, *J. Quant. Spec. Rad. Trans.* **54**, 767 (1995).
- ⁸⁵J. Huennekens, "Collisional and radiative processes in sodium vapor," Ph.D. dissertation (University of Colorado, 1982) (unpublished).
- ⁸⁶C. M. Wolfe, "Collisional transfer of population and orientation in NaK," Ph.D. dissertation (Lehigh University, 2010) (unpublished).
- ⁸⁷P. Andresen, H. Joswig, H. Pauly, and R. Schinke, *J. Chem. Phys.* **77**, 2204 (1982).
- ⁸⁸A. V. Smith and A. W. Johnson, *Chem. Phys. Lett.* **93**, 608 (1982).
- ⁸⁹R. Fei, H. M. Lambert, T. Carrington, S. V. Filseth, C. M. Sadowski, and C. H. Dugan, *J. Chem. Phys.* **100**, 1190 (1994).
- ⁹⁰S. Antonova, K. Urbanski, A. M. Lyyra, F. C. Spano, and L. Li, *Chem. Phys. Lett.* **267**, 158 (1997).
- ⁹¹C. W. McCurdy and W. H. Miller, *J. Chem. Phys.* **67**, 463 (1977).
- ⁹²M. M. Maricq, *J. Chem. Phys.* **103**, 5999 (1995).
- ⁹³S. Ashman, B. McGeehan, C. M. Wolfe, C. Faust, K. Richter, J. Jones, A. P. Hickman, and J. Huennekens, "Experimental studies of the NaCs $5^3\Pi_0$ and $1(a)^3\Sigma^+$ states" (unpublished).
- ⁹⁴B. Kamke, W. Kamke, K. Niemax, and A. Gallagher, *Phys. Rev. A* **28**, 2254 (1983).